Aerodynamic gradient flux measurements of ammonia in intensively grazed grassland: temporal variations, environmental drivers, methodological challenges and uncertainties

Mubaraq Olarewaju Abdulwahab[1], Christophe Flechard[1], Yannick Fauvel[1], Christoph Häni[2], Adrien Jacotot[1,a], Anne-Isabelle Graux[3], Nadège Edouard[3], Pauline Buysse[1], Valérie Viaud[1], Albrecht Neftel[4]

[1]UMR 1069 SAS, INRAE, Institut Agro, Rennes, 35042, France
[2]School of Agricultural, Forest and Food Sciences HAFL, Bern University of Applied Sciences, Zollikofen, 3052, Switzerland
[3]UMR PEGASE, INRAE, Institut Agro, Saint-Gilles, 35590, France
[4]Neftel Research Expertise, Wohlen b. Bern, 3033, Switzerland
[a]now at: CarboFlux, France

Correspondence to: Mubaraq Olarewaju Abdulwahab (mubaraq-olarewaju.abdulwahab@inrae.fr)

Abstract. Understanding the factors controlling surface-atmosphere exchange of ammonia (NH_3) in grazed grasslands is crucial for improving atmospheric models and addressing environmental concerns associated with reactive nitrogen. However, in-situ micrometeorological NH_3 flux measurements in pastures remain scarce in the literature. This study presents high-resolution NH_3 flux data collected during four spring campaigns (2021 – 2024) at an intensively managed grassland site in Northwestern France, using the aerodynamic gradient method (AGM) alongside continuous monitoring of environmental variables and agricultural management. AGM-derived NH_3 fluxes exhibited distinctive patterns: (i) high variability during grazing from -113 (deposition) to +3205 (emission) ng NH_3 m^{-2} s^{-1}, influenced by meteorology, grazing livestock density, and vegetation and soil dynamics; (ii) strong diurnal patterns and day-to-day variability; and (iii) transient volatilisation peaks following slurry applications (up to 10235 ng NH_3 m^{-2} s^{-1}). Grazing-induced fluxes often persisted for up to 1-2 weeks following cattle departure. Relative random uncertainties associated with AGM flux measurements ranged from typically 15% to 70%, based on errors in vertical concentration gradient slopes and variables related to turbulence and stability. Additional methodological limitations and systematic uncertainties are discussed, in particular errors associated with fundamental AGM assumptions and flux footprint attribution in a rotational grazing setup. Emission factors (EF), calculated for NH_3 derived from deposited cattle urine nitrogen, varied considerably between grazing events, from 1 to 23 g NH_3-N cow^{-1} grazing d^{-1}, reflecting the interplay between livestock management and environmental factors. This study highlights the importance of long-term, continuous, high-resolution measurements to document the large variability in grazing-induced NH_3 fluxes. The findings also underscore the need for refining bi-directional exchange models that integrate physics (meteorology, turbulence), environmental biogeochemistry (the fate of excreted nitrogen in the soil), biology (dynamic vegetation processes), and pasture management (grazing intensity) in grazed grassland systems.

1 Introduction

Agriculture is the largest global source of NH$_3$ emissions, accounting for 94% of total emissions in the European Union, with
35 livestock agriculture contributing 72% (EEA, 2022). Globally, grazing and livestock feed production, which utilize 67% of
agricultural land, contribute significantly to the agricultural sector accounting for 40-50% of gross domestic product but also
generate substantial NH$_3$ emissions due to intensive management practices aimed at enhancing productivity (FAO, 2023;
Hristov et al., 2011; Salmon et al., 2020). These emissions contribute to fine particulate matter (PM$_{2.5}$) formation, biodiversity
loss, eutrophication, and broader consequences for ecosystem health (Asman et al., 1998; Sutton et al., 2011). Additionally,
40 dry-deposited NH$_3$ influences nitrogen cycling by promoting nitrification and denitrification processes that contribute to
nitrous oxide (N$_2$O) emissions (Skiba et al., 2005), a potent greenhouse gas with ozone-depleting properties (Forster et al.,
2021).

In grazed grasslands, NH$_3$ emissions originate primarily from nitrogen (N) in livestock excreta, deposited during grazing, and
also from N applied as synthetic fertilizers and organic manures, such as cattle slurry, to sustain pasture growth. Urine, rich in
45 urea, serves as the principal NH$_3$ source, with urease enzymes facilitating urea hydrolysis (Whitehead and Raistrick, 1993).
Ammonia emissions per unit area are comparatively lower in grazing systems than in confined animal feeding operations
(CAFOs) due to urine infiltration into the soil and reduced excreta accumulation in housing areas. As a result, continuous
grazing can potentially halve total annual emissions in dairy systems compared to CAFOs (Sutton et al., 2022). However, the
overall mitigation impact depends on the grazing duration, housing hygiene and the associated trade-offs with other N losses
50 such as nitrate leaching and N$_2$O emissions. Moreover, NH$_3$ emissions from grazing are still crucial given the extensive land
area, increasing livestock densities and excreta deposition on pastures (Sutton et al., 2022).

Ammonia volatilisation, i.e. the shift from aqueous-phase ammonium (NH$_4^+$) to gas-phase NH$_3$ and transfer to the atmosphere,
is highly dynamic and influenced by environmental and management factors, including temperature, canopy structure, soil
moisture, and relative humidity, with emissions increasing under higher pH and warm conditions (Freney et al., 1983). The
55 interactions between management practices, soil, and meteorology create substantial temporal and spatial variability in NH$_3$
fluxes (Flechard et al., 2013; Sommer et al., 2003), which are poorly understood in grazing systems. Emission factors (EF)
represent the amount of nitrogen emitted per activity unit (e.g., the fraction of applied N, or the emission per cow per day)
released as NH$_3$. Therefore, they exhibit significant variability depending on the same control factors. While EFs for
fertilization-induced NH$_3$ emissions are well-documented, grazing-related NH$_3$ fluxes remain poorly characterized due to
60 scarce in-situ micrometeorological measurement datasets. Most existing NH$_3$ EF estimates for grazing are often based on short-
term studies, or artificial conditions, limiting their applicability for long-term assessments and modelling efforts (Bell et al.,
2017; Sommer et al., 2019; Voglmeier et al., 2018).

Micrometeorological techniques such as the aerodynamic gradient method (AGM) and eddy covariance (EC) have been
commonly used for field-scale NH$_3$ flux measurements. The AGM estimates fluxes indirectly, based on vertical concentration
65 gradients, turbulence measurements and Monin-Obukhov similarity theory, applying K-theory within the atmospheric surface

layer (Monteith and Unsworth, 1990). It has been widely used in several ecosystems including moorlands (Flechard and Fowler, 1998), crop fields (Loubet et al., 2012), and grasslands (Flechard et al., 2010; Milford et al., 2001; Wichink Kruit et al., 2007), often in combination with wet chemical instrumentation (e.g., Loubet et al., 2012), though optical systems are becoming more prevalent (Kamp et al., 2020). In contrast, EC provides direct, high-temporal-resolution measurements of NH_3

70   fluxes using rapid-response (> 5 Hz) analysers correlated with high-frequency wind velocity data (Famulari et al., 2005). However, both methods face similar challenges. The soluble, reactive and adhesive properties of NH_3 complicate concentration measurements, as adsorption and desorption on sampling surfaces (e.g., inlet tubing, filters) can introduce biases (Nemitz et al., 2004; Ellis et al., 2010; Schulte et al., 2024; Whitehead et al., 2008). Recent advancements in open-path analysers EC systems have mitigated these limitations for both AGM and EC (Swart et al., 2023).

75   Micrometeorological methods require in principle footprint homogeneity, steady-state turbulence, and minimal advection, which are difficult to maintain under real field conditions (Mauder et al., 2021). Despite these challenges, studies have demonstrated reasonable agreement between AGM and EC measurements, making them valuable tools for monitoring NH_3 flux dynamics (Swart et al., 2023), and other chemical species such as ozone (Loubet et al., 2013) and fumigants (Anderson et al., 2019). Alternative approaches, such as backward Lagrangian stochastic (bLS) modelling, have been shown to provide

80   robust NH_3 emission estimates in controlled conditions by accounting for the geometry of the source (Häni et al., 2024). However, bLS accuracy remains sensitive to meteorological inputs and dispersion assumptions (Kamp et al., 2021), and systematic differences between dispersion models up to 60%, depending on the turbulence scheme, have been reported in the literature (Carozzi et al., 2013).

The inherent complexity associated with micrometeorological methods necessitates extensive instrumentation and

85   maintenance (Harper, 2005), thus increasing measurement costs and contributing to the scarcity of high-frequency, continuous NH_3 flux data and the large uncertainty in EFs estimates (Sommer et al., 2019). Understanding the variability and drivers of grazing-induced NH_3 emissions under different conditions is crucial for improving process-based models, their eventual implementation in chemical transport models (CTMs), and EF estimates. Process-based models depend on accurate high-resolution measurements to improve surface-atmosphere NH_3 exchange parameterizations, which are essential for predicting

90   atmospheric composition, air quality improvement, assessing budgets and informing policies (Massad et al., 2020; Sutton et al., 2013)

In this study, we present multi-year, high-resolution NH_3 flux field-scaled measurements collected using the AGM with a closed path quantum cascade laser NH_3 analyser during four consecutive spring campaigns at an intensively grazed grassland monitoring site in NW France. To our knowledge, this dataset is one of the longest of its kind for NH_3 fluxes in pastures, which

95   makes possible the investigation of NH_3 emissions over several grazing events, in contrasting weather and environmental conditions. Specifically, we aim to (i.) quantify the temporal (diurnal, day-to-day, seasonal) dynamics of NH_3 fluxes associated with grazing activities, (ii.) investigate the relationship between environmental factors and NH_3 fluxes and (iii) evaluate uncertainties and methodological limitations of in-situ AGM measurements in grazed grasslands.

2 Materials and methods

2.1 Site description

Ammonia flux measurements were conducted at the Integrated Carbon Observation System (ICOS) FR-Mej station (https://meta.icos-cp.eu/resources/stations/ES_FR-Mej), located at the Mejusseaume dairy experimental research facility of the French National Research Institute of Agriculture, Food and Environment (INRAE, IEPL, 35650 Le Rheu, France; https://doi.org/10.15454/yk9q-pf68). The site, located about 10 km west of the city of Rennes, NW France is situated at 48°7'6"N 1°47'48"W with an altitude of 35 meters above mean sea level. The soil is classified as a stagnic/luvic Cambisol with a sandy clay loam texture (20 % clay, 47% silt and 33% sand). The topsoil (0-30 cm) has a near-neutral pH (6.5, measured by 1 mol l^{-1} KCl) with an average bulk density of 1.36 Mg m^{-3}. The predominant wind direction during spring measurements in 2021-2024 was from the NW and SW directions; the main farm buildings are located to the SE (Fig. 1). The 4.7-hectare field is managed as a pasture sown with ryegrass (*Lolium perenne L.*) with a transition to silage maize cropping for one season (May to September) every 5 to 6 years.

This setup supports rotational grazing, with livestock grazing 4-6 times per year, including 2-4 phases concentrated in the spring when grass growth is vigorous. The dairy herd consists of the Holstein breed which typically grazes 18-20 hours each day, with feed supplementation provided during milking hours. The field is usually separated into two halves for grazing, i.e., NW (Plot A) and SE (Plot B) halves, each 2.35 hectares. A fence running from NNE to SSW bisects the area, facilitating rotational grazing across the two plots (Fig. 1).
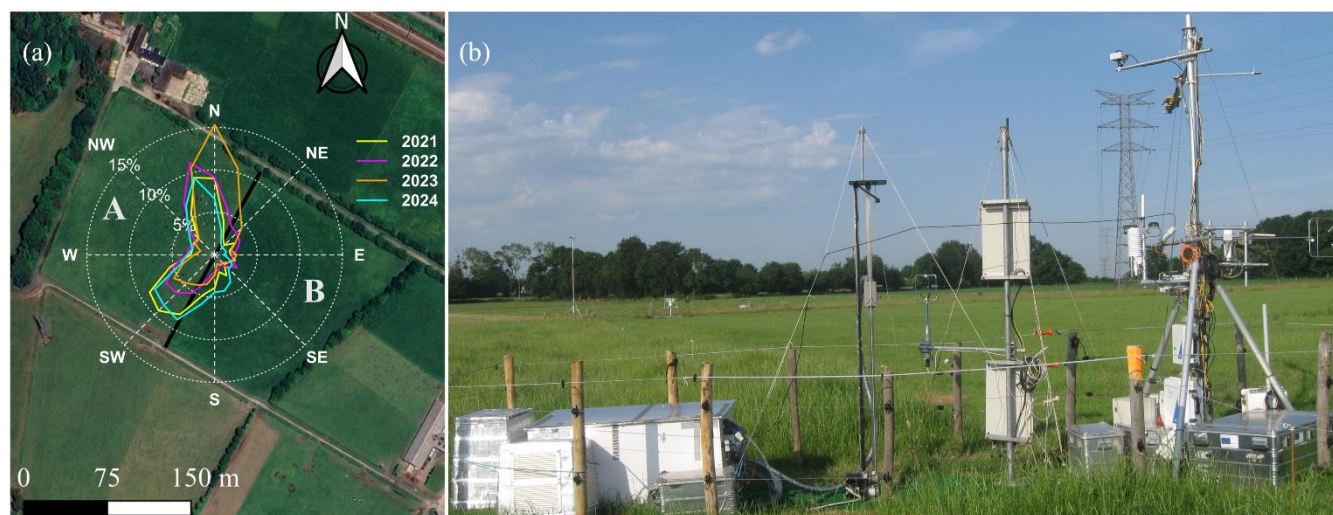
Figure 1: (a) Aerial view of the study area showing plot A (NW) and plot B (SE), with the fence shown as a black line, and the windrose indicating prevailing wind directions during the spring campaigns of 2021–2024 (© Google Maps 2025, mapped in QGIS software). (b) Field instrumentation setup, including the vertical NH₃ gradient profiling (mechanical lift) system, wind and turbulence sensors (3-D ultrasonic anemometers) and meteorological station.

2.2 Measurement periods and management events

Flux measurements were conducted during spring campaigns from 2021 to 2024. Measurement periods varied across years: May-June in 2021, April-June in 2022 and 2023 and March-early July in 2024, capturing key management activities. Grazing

125 did not occur simultaneously in both plots but rather in succession, requiring the two plots to be treated as distinct entities (Sect. 2.1). Stocking density varied from 16 to 55 LSU ha^{-1} across the 4 years. Fertilization events with flux data coverage included two applications in 2022 (39 kg NH$_4$NO$_3$-N ha^{-1} on 19/04 and 53 kg N ha^{-1} as cattle slurry on 31/05), one in 2023 (39 kg NH$_4$NO$_3$-N ha^{-1} on 28/04), and one in 2024 (25 kg NH$_4$NO$_3$-N ha^{-1} on 6/05). For this paper, we focus on ten grazing events where data availability was reasonable to evaluate flux responses under grazing conditions. Details on stocking density, flux

130 quality, and data coverage for these events are summarized in Table 2.

2.3 Instrumentation: AGM flux measurements and meteorological data collection

The surface-atmosphere NH$_3$ exchange fluxes were measured during spring grazing (June 2021 - June 2024) using a modified hybrid version of the aerodynamic flux-gradient method (AGM) as described in Flechard and Fowler (1998). By contrast to the original full AGM described in earlier studies (Fowler and Duyzer, 1989), a 3-D ultrasonic anemometer was used here to

135 measure friction velocity (u*) and sensible heat flux (H), instead of wind and temperature vertical profiles.

2.3.1 Micrometeorology theory

The AGM relies on empirical relationships between turbulent fluxes and mean vertical gradients of NH$_3$ concentration (χ) above the surface (Monteith and Unsworth, 1990; Thom, 1975). This approach relies solely on measured vertical concentration profiles in situ on the field, with no measurement of the concentration profile upwind of the field. Following Fick's first law,

140 whereby a diffusive flux equals the product of a diffusion coefficient and a scalar concentration gradient, and based on the Monin-Obukhov similarity theory, the turbulent NH$_3$ exchange flux between the surface and the atmosphere is described as the product of eddy diffusivity for heat and trace gases (K$_H$) and the vertical concentration gradient (dχ/dz) measured in the inertial sublayer:

$$F_\chi = -K_H \frac{d\chi}{dz} \tag{1}$$

145 where z is the height above the ground. By convention, the negative sign implies that emission is positive and deposition is negative. The flux F_χ is assumed to be constant with height, under conditions of sufficient and homogeneous upwind fetch, stationarity (dχ/dt ~0), negligible horizontal advection (dχ/dx ~0), and negligible chemical sources and sinks in the air column below the maximum measurement height. However, both K$_H$ and dχ/dz depend on height, limiting the practical implementation of Eq. (1). Sutton et al. (1993) demonstrated that equation (1) could be simplified as the product of two height-independent

150 variables, friction velocity (u$_*$) and a trace gas concentration-scaling parameter (χ_*) such that:

$$F_\chi = -u_* \chi_* \tag{2}$$

with

$$\chi_* = -k \frac{d\chi}{d[ln(z-d) - \psi_H\left(\frac{z-d}{L}\right)]} \tag{3}$$

where k is the von Karman constant (0.41), d is the displacement height of vegetation or other roughness elements, L is the
155   Obukhov length, and ψ_H is a height-integrated stability correction function, which accounts for the distortion effects of
atmospheric stability or instability on the shape of scalar logarithmic profiles in the inertial sublayer (Panofsky, 1963; Paulson,
1970). In neutral and stable conditions it is assumed that eddy diffusivities for momentum, heat and trace gases are equal;
further, in stable conditions ψ_H and the equivalent stability correction for momentum (ψ_M) are equal (Webb, 1970) such that:

$$\psi_H\left\{\frac{z-d}{L}\right\} = \psi_M\left\{\frac{z-d}{L}\right\} = -5.2\frac{z-d}{L} \tag{4}$$

160   For unstable conditions, the height-integration of the Dyer and Hicks (1970) similarity function for heat and trace gases was
provided by Paulson (1970):

$$\psi_H\left\{\frac{z-d}{L}\right\} = 2ln\left(\frac{1+x^2}{2}\right) \tag{5}$$

with

$$x = \left(1 - 16\frac{z-d}{L}\right)^{1/4} \tag{6}$$

165

2.3.2 Vertical profile concentration measurement system

The AGM was implemented using a gradient-lift ammonia sampling system (GLASS). The GLASS consisted of a
concentration profiling setup with up to 5 measurement heights (0.1, 0.2, 0.5, 1.1, and 2.1 m) above the ground. A single
heated, insulated 3 m long PFA inlet line (1/2'' o.d., 3/8'' i.d), was sequentially and continuously lifted up, then lowered down,
170   a vertical mast using a winch and pulley, conveying the air sample to an NH_3 analyser. This single, vertically mobile inlet line
with a large sampling flow rate was used to minimize potential concentration biases between different heights that may
otherwise result from using several tubes associated with a set of solenoid valves. The lift system was custom-designed and
built at the INRAE-IEPL workshop (Méjusseaume, Le Rheu, France) and was controlled, and all data acquisition and
processing was performed, by a CR6 datalogger (Campbell Scientific Inc, Logan, UT, USA). The sampling height followed a
175   200-s sampling sequence from bottom to top, idling several tens of seconds at each of the 3 to 5 designated sampling heights
for concentration to stabilize, then moving on to the next height, with around 50 s of discarded integrated travelling time
(unused for gradient determination) per 200-s cycle.

2.3.3 Air sampling and ammonia detection

The air sample was drawn into the ammonia analyser using an Edwards XDS-35i dry scroll pump (Edwards Ltd, Burgess Hill,
180   West Sussex, UK) placed downstream of the measurement cell. An auxiliary pump (KNF model N940, KNF Neuberger

GmbH, Freiburg, Germany) with a flow rate of 25 slpm was attached to a T-junction connecting the main sampling line to the 'sample IN' port of the analyser; this auxiliary pump increased the airflow up to 35 slpm in the inlet line (before the entry point into the analyser), helping reduce the residence time of the sample and signal attenuation associated with potential NH_3 adsorption to inner surfaces of the PFA tube.

185   The sampling head was fitted with a Teflon©-coated aluminium cyclone to remove coarse aerosols from the air sample (model URG-2000-30EHB, URG Corp, Chapel Hill, NC, USA), with a nominal 1 µm cut-off point for a 16.7 slpm sampling rate. The only filter in the NH_3 sampling system was a 47-mm diameter, 1.2-µm pore size PTFE filter located inside the analyser, which was required to preserve the very large mirror reflectivity inside the optical cavity. Ammonia concentrations were measured at 1 Hz resolution/integration time by a Los Gatos Research off-axis, integrated cavity output spectroscopy (OA-ICOS)

190   quantum cascade laser (QCL) analyser (model LGR-FTAA, Fast Trace Ammonia Analyser, ABB/LGR group, San Jose, CA, USA). The nominal precision (1-σ) of the QCL analyser was 0.2 ppb at a 1-s integration time; the instrument was similar, though not identical, to the model described by Leen et al. (2013). Notable differences in our analyser included a larger critical orifice (1.7 mm), a larger sampling rate through the cell (10 slpm) using a different pump, and a lower cell pressure setpoint (100 Torr).

195   **2.3.4 Gradient concentration data processing and corrections**

When AGM flux measurements are conducted with a single concentration detector measuring non-simultaneously at two or more heights above the surface (sequential sampling), the vertical gradient may be biased (high or low) due to non-stationarity in the air mass, if temporal concentration changes ($d\chi/dt$) are significant during the interval it takes to sample a full vertical profile (Fowler and Duyzer, 1989; Kamp et al., 2020). To minimize biases on the measured flux, we applied a linear

200   concentration detrending procedure for individual height measurements based on the concentration change between two consecutive cycles of the lift sampling system. The concentration profiles were processed using half-hourly averaging. Only the last 5 seconds of the concentrations measured during the 30-50 seconds of stabilization time at each sampling height (before the sampling head moved to the next position) were used in the final concentration averaging. The stabilization time was implemented to reduce memory effects from the previous height since NH_3 is known to stick to inner sampling surfaces (tubes,

205   filters, cell) of closed path measurement systems. Nine 200-s sampling cycles were performed, then averaged, within each half-hour, which was the time resolution for turbulence and flux calculation and averaging. An example of the resulting half-hourly time series of the GLASS LGR-FTAA NH_3 concentration profile is shown in Fig. 3.

As no reliable gas-phase calibration system was available to check or calibrate the LGR-FTAA instrument in the ambient concentration range encountered in the field, we used an indirect, *a posteriori* correction method based on a comparison with

210   another, co-located, absolute NH_3 sampling method (DELTA® denuder system, see procedure described in 2.3.5) placed within 1 m distance at the same height of the mast midpoint (1.1 m above ground). AGM fluxes were computed utilizing Eq. (2) with the slope of the stability-corrected vertical concentration gradient (χ_*) calculated by a linear least-square regression

of χ versus the quantity ln(z-d) - ψ_H{(z-d)/L} (Eq. 3); by default, the flux calculations presented in the paper were made with concentrations measured from 0.5 m up to 2.1m above the surface.

2.3.5 Dry Denuder Sampling for Ammonia Concentration Reference

To provide a reference and correction for NH_3 concentration measurements made by the QCL instrument, we used UKCEH DELTA® denuder measurements (DEnuder for Long-Term Atmospheric sampling; https://www.ceh.ac.uk/solutions/equipment/air-sampler-systems-environmental-monitoring). The DELTA® system is a low-cost diffusion-based dry denuder, originally designed for long-term NH_3 sampling (Sutton et al., 2001). It operates on the principle of a single-bore glass denuder for sampling trace gases (Ferm, 1979), where a laminar air stream passes through the denuder coated on the inside with an acid solution (e.g., citric acid). The acid walls capture gas-phase NH_3 to be later extracted in the laboratory, while slower-diffusing, NH_4^+ -containing aerosols pass through and are collected by aerosol filters placed downstream of the denuder. Air is drawn through the denuder at 0.3-0.4 l min^{-1}, ensuring very efficient NH_3 scrubbing while allowing aerosols separation.

In this study, DELTA® denuders were deployed in the field at a height of 1.1 m, co-located and aligned with the mid-point of the NH_3 gradient mast. After exposure, the denuders were analysed for ammonium (NH_4^+) content using continuous flow analysis (CFA) and spectrometric detection following ISO 11732:2005. With a near-100% capture efficiency for gas-phase NH_3 and a high-precision total (time-integrated) flow measurement, the DELTA® system is expected to yield a near-absolute mean NH_3 concentration over an exposure period. The DELTA® system was originally tuned for long-term concentration monitoring, with typically monthly sample change-over frequency, but shorter and longer periods are also possible, depending on ambient concentrations. Here, we used much shorter exposure intervals of typically 1-3 days during grazing and fertilization events and 1-2 weeks during background phases to increase the number of comparison points with the QCL instrument. These DELTA® NH_3 concentration data were then used to correct *a posteriori* the whole LGR-FTAA NH_3 concentration dataset, using linear regressions of the DELTA® data points versus the mean LGR-FTAA concentrations computed for each of the DELTA® sampling intervals (see Fig. 2).

2.3.6 Meteorological and ecosystem data

Micro-meteorological data were collected to characterize turbulence and support NH_3 flux computations using equations (2) and (3). Turbulence variables, including friction velocity (u∗, m s^{-1}) and Obukhov length (L, m), were calculated using the Eddypro software (v 7.0.9, LI-COR Biosciences, Lincoln, NE, USA) from 10 Hz raw data measurements using a 3-D ultrasonic anemometer (HS-50, Gill Instruments Ltd., UK) mounted at a height of 2 m. Additional meteorological variables included precipitation (tipping bucket rain gauge, ARG314, Campbell Scientific), air temperature, relative humidity and vapour pressure deficit VPD (HMP155 Humicap probe, Vaisala GmbH, Germany), global and net radiation (CNR4 net radiometer, Kipp and Zonen, NL), and soil temperature (time domain reflectometry probe CS650, Campbell Scientific, USA). All these were

measured at sub-minute intervals and averaged over 30-minute intervals. Ecosystem-related variables included biomass
245 (measured with a strip mower), canopy height (measured using a herbometer) and leaf area index (LAI, measured using the
Sunscan probe (model SS1) and BF5 sunshine sensor, DELTA-T Devices Ltd, UK). Bulk N content of vegetation was also
measured before grazing. Soil pH and nitrogen dynamics (see methods in Sect. S1 of the supplement) were also monitored.
These measurements enabled capturing both changes in vegetation structure and soil characteristics, which are essential to
understanding ecosystem processes driving NH_3 emissions.

2.4 Flux data processing, corrections and quality control procedures

To ensure the integrity and quality of flux measurements, the following procedures were applied.

2.4.1 Storage flux correction

Temporal variations in NH_3 storage within the air column below the mean measurement height of the gradient system (z_{mean} =1.1 m) were considered. For NH_3, where exchange fluxes are significantly large compared to concentration, the flux
255 divergence attributed to storage change is typically considered negligible as mentioned by Sutton and Fowler
(1992). Nevertheless, the error in the flux due to storage (F_{sto}) was systematically calculated from:

$$F_{sto} = \int_0^{z_{mean}} \frac{\partial \chi}{\partial t} dz \qquad (7)$$

2.4.2 Footprint attribution

Since there was only one flux measurement setup on the field, differences in management practices between adjacent plots
260 necessitated precise footprint attribution, especially under rotational grazing and frequent changes in wind direction. The
Kormann and Meixner (2001) footprint model was employed to calculate the contributions of specific field areas to the
measured fluxes, namely from plot A, the primary footprint sector from SW through NW winds, and plot B for fluxes under
NE through SE wind directions (Fig. 1). For time intervals when plots A and B were under differential management, i.e. one
plot was grazed or fertilized while the other was not, a minimum footprint contribution of 2/3 (66.67%) was required for the
265 measured flux to be considered representative of the plot of interest. Fluxes for which footprint contributions from either plot
were less than the 2/3 threshold were discarded (for the plot of interest). If the 2/3 footprint threshold was exceeded in one
plot, the flux was validated and then corrected for the background interference from the fraction of footprint outside the plot
of interest (see Sect. 2.4.5). For time intervals when plots A and B were under the same management (e.g., fertilization of the
whole field), both plots were assumed to have similar flux levels and thus no footprint correction was applied.

2.4.3 Filtering of flux measurements

The flux data were further filtered to exclude flux measurements that did not meet steady-state, fully developed turbulent conditions and stationarity for momentum, sensible heat and trace gas fluxes.

a. Momentum and sensible heat flux screening: the quality flagging system by Mauder and Foken (2004) was applied to EC fluxes of momentum (qc_τ) and sensible heat (qc_H), to ensure adequate quality of EC-derived friction velocity (u*) and sensible heat flux (H) for the purpose of AGM flux calculations. Their 0-1-2 flagging policy is now a de facto standard in networks such as ICOS, AmeriFlux and FLUXNET. "0" means high-quality fluxes, "1" means fluxes are suitable for budget analysis, "2" means fluxes that should be discarded from the resulting dataset due to bad quality. The overall flag is determined as a combination of a steady state test (compares the statistical parameters determined for the averaging period and for short intervals within this period, with score 1-9), and an integral turbulence characteristics test (verifies whether the ratio of the standard deviation of a turbulent parameter to its turbulent flux is nearly constant or a function of stability, with score 1-9). Measurements flagged as 2 by the Eddypro® software (v7.0.9) were excluded while flags of 0 and 1 (combinations of qc_τ/qc_H 0/0, 0/1, 1/0, 1/1) were deemed acceptable and retained.

b. NH_3 stationarity: a $qc_{NH3\ stationarity}$ quality flag was devised to assess the stationarity of NH_3 concentrations over 30-minute intervals, based on the coefficient of variation (CV) of NH_3 concentrations measured over the nine vertical lift ascents within each half-hour. A flag of 2 was assigned to data where the CV exceeded 100% indicating high variability and non-stationary conditions, unsuitable for flux calculations. Data with CV values < 10% were flagged as 0, while values between 10% and 100%, were flagged as 1 and retained.

c. Stability parameter: fluxes were filtered based on the stability parameter $\zeta = (z_{mean}-d)/L$, where z_{mean} is the mean measurement height of the profile system (1.1 m). This filter excluded extreme stability conditions where the flux-gradient relationship deteriorates and stability corrections become less reliable. Data with ζ values outside predefined thresholds (<-0.5 or > 0.2), were flagged as 2 and excluded. Data within the -0.2 to 0.05 were flagged as 0 (best quality because due to proximity to atmospheric neutral stability), while values between -0.5 and -0.2 (moderately unstable) or between 0.05 and 0.2 (moderately stable) were flagged as 1 and further retained.

d. Micrometeorological screening; the overall micrometeorological score $qc_{\mu met}$ was determined by combining the maximum flag scores of qc_τ, qc_H, qc_L and $qc_{NH3\ stationarity}$. Half-hours with a score of 2 were excluded and only measurements meeting all individual screening criteria (0 or 1) were retained for further flux analysis, ensuring high data quality for AGM flux computations.

2.4.4 Classification of flux quality

300 The fluxes were categorized according to micrometeorological screening scores and footprint contribution as shown in Table 1.

Table 1: Quality classification of validated NH₃ flux measurements based on micrometeorological screening (qc_{μmet}) and footprint contribution criteria. qcA: best quality; qcB: good quality; qcC: modest quality fluxes.

qc_{μmet}	Footprint (%)			
	<66.7	66.7-80	80-90	>=90
0	reject	qcC	qcB	qcA
1	reject	qcC	qcC	qcB
2	reject	reject	reject	reject

305

2.4.5 Corrections for background flux interference

During grazing on the plot of interest (whether A or B, depending on the date), corrections were applied to account for the potential 'dilution' of the targeted emission fluxes by background fluxes from adjacent (ungrazed) plots, in cases where there was an overlap in the measurement footprint. Since the threshold for footprint validation was 2/3 for the plot of interest, up to

310 1/3 of the flux footprint was potentially located in an adjacent plot, which we assumed to be in a state of background flux, i.e. a small or near-zero emission or deposition (see e.g., Flechard et al., 2010). The measured flux (F_{meas}) was therefore adjusted using a simple canopy compensation point model approach to estimate the background flux (F_{bgd}) (see supplement S14) over adjacent fields, based on resistance modelling and environmental conditions (Massad et al., 2010; Nemitz et al., 2001). The grazed field fluxes (F_g) were adjusted following Eq. 8-9, to ensure that flux values more accurately reflected true emission

315 fluxes on the grazed field. Such corrections are tentative since the true background flux of the adjacent plot is not known and estimated using a modelling approach, but the absence of such correction would very likely underestimate the actual emission by grazing.

In practice, we assumed that the net measured flux (F_{meas}) was comprised of the two components F_g and F_{bgd} weighted by their respective percentage footprint contributions FP_g and FP_{bgd}, such that:

320
$$F_{meas} = F_g \times FP_g + F_{bgd} \times FP_{bgd} \tag{8}$$

The corrected flux for the grazed plot (F_g) was then calculated as:

$$F_g = \frac{(F_{meas} - F_{bgd} \times FP_{bgd})}{FP_g} \tag{9}$$

These corrections were applied only for positive (emission) fluxes measured in the grazed field, and when the nearby fields were assumed not to be emitting due to observed management activities. When grazing occurred in close succession across

325 both fields, no corrections were deemed necessary, as grazing-induced fluxes were assumed to be more or less consistent across the entire field, thus negating the need for additional adjustments.

2.5 Uncertainty analysis

For AGM-derived fluxes, the random standard error of the half-hourly NH_3 fluxes ($SE(F_{meas})$) was estimated following standard error propagation rules as the square root of the sum of the squares of the fractional errors associated with each key component

330 of Eq. 2:

$$\frac{SE(Fmeas)}{|Fmeas|} = \sqrt{\left(\frac{SE(u*)}{u*}\right)^2 + \left(\frac{SE(\chi^*)}{\chi^*}\right)^2} \tag{10}$$

where the components are:

      i)   Random error of friction velocity ($SE(u_*)$)

The random error in u* was derived from the random error of the momentum flux (τ), calculated as:

335 $$SE(u*) = \frac{SE(\tau)}{2\rho u*} \tag{11}$$

where $SE(\tau)$ is the random standard error of the momentum flux, estimated using EddyPro v7.0.9 following Finkelstein and Sims (2001), and ρ is the air density. This error estimation method first requires the preliminary estimation of the integral turbulence time-scale (ITS), which can be defined as the integral of the cross-correlation function; the next step is based on the calculation of the variance of covariance (see Eq. 8 in Finkelstein and Sims, 2001)

340   ii)   Random error of the NH_3 vertical gradient term ($SE(\chi^*)$)

The uncertainty associated with the stability-corrected vertical concentration gradient was estimated as the standard error of the slope of the linear regression of NH_3 concentration (χ) vs $[ln(z - d) - \psi_H\left(\frac{z-d}{L}\right)]$.

2.6 Gap-filling approach and cumulative flux estimation from mean diurnal variation analysis

To estimate cumulative NH_3 emissions and grazing cattle EF, gaps in half-hourly time series of measured fluxes were filled

345 using a statistical approach based on mean diurnal variations, in which mean diurnal cycles are calculated from the available flux data over several days of measurements, and missing fluxes at a certain time of day are assumed to equal the matching

value from the mean diurnal cycle. A diurnal approach was necessary since flux patterns exhibited very strong differences between day and night (see Results).

However, this approach may lead to biased results if few flux data are available at certain times of the day, or especially at
350 night when low wind speed and suppressed turbulence often lead to flux data rejection, and if outliers bias the calculated arithmetic mean of a small population. In addition, the very strong day-to-day dynamics in mean daily fluxes, and short-lived but very large peaks within a single grazing event, can also lead to biased mean diurnal cycles calculated over the whole grazing period. To reduce the risk of large biases associated with such temporal features, mean diurnal flux patterns were calculated in two stages:

355 1- Each corrected flux for the grazed plot (F_g) at hour "H" on the day "D" was divided by (normalized to) the maximum flux of that day:

$$F'(H,D) = \frac{F_g(H,D)}{F_{dailyMax}(D)} \quad (12)$$

2- A mean diurnal cycle of the normalized dimensionless fluxes (F') was calculated from all available data over the grazing period. The normalized mean diurnal profile of F'$_{avg}$(H) thus varied between ~0 and 1.

360 The gap-filled flux (F_{gf}) for each missing flux value at hour H on day D was subsequently calculated as the product of the $F'_{avg}(H)$ value, looked up from the normalized mean diurnal cycle, by the maximum measured flux on day D:

$$F_{gf}(H,D) = F'_{avg}(H) \times F_{dailyMax}(D) \quad (13)$$

This method is subsequently referred to as the mean diurnal variation normalized to the maximum (DVmax). A variant of the same method was also implemented, whereby the fluxes were normalized to the daily average flux (DVavg) instead of the
365 daily maximum. A graphical illustration of the steps involved in the calculation method is provided in Figure S10 (Supplement). For grazing events (e.g., G9 and G10), where flux data were missing on some days (due to the quality filtering), a modified gap-filling approach was applied to maintain consistency with the DVmax/DVavg framework (see Sect. S2 in the supplement).

3 Results

370 ### 3.1 Correction of QCL NH₃ concentration data using DELTA® denuders

Linear regressions between time-integrated DELTA® concentrations and average LGR-FTAA concentrations over corresponding time intervals are shown in Fig. 2a based on simultaneous sampling at 1.1 m above ground during the spring campaigns of 2022-2024. The relationships between the two measurement methods were highly linear (all R^2 values above 0.97) and fairly consistent over nine monthly periods, but with significant slopes (mean 1.5, range 1.3 – 1.8) and offsets (mean
375 -1.7, range -0.1 to -4.3 µg m^{-3}). The variability in regression slopes resulted from different degrees of cleanliness and reflectivity of mirrors inside the LGR-FTAA optical cavity, affecting transmitted laser intensity levels and, as a result, absolute concentration outputs, hence the need for differential corrections at different times. Prolonged high-flow sampling in the field

resulted in the gradual accumulation of fine aerosol matter on the LGR-FTAA mirrors, which were cleaned with acetone and methanol once or twice per spring campaign to restore mirror reflectivity. Freshly cleaned optics resulted in a smaller

380   regression slope, i.e. a smaller correction was required.

Over the range of mean NH_3 values measured by time-integrated DELTA® over relatively short intervals of typically one to several days (range 1 to 31 µg m^{-3}; Fig. 2b), the magnitude of the resulting concentration correction was generally relatively small up to 5 µg m^{-3}, because the effect of the slope of typically 1.4-1.6 was more or less cancelled out by the negative offset of 1-2 µg m^{-3}. At larger concentrations, the effect of the slope dominated, resulting in much larger corrections.

385

390
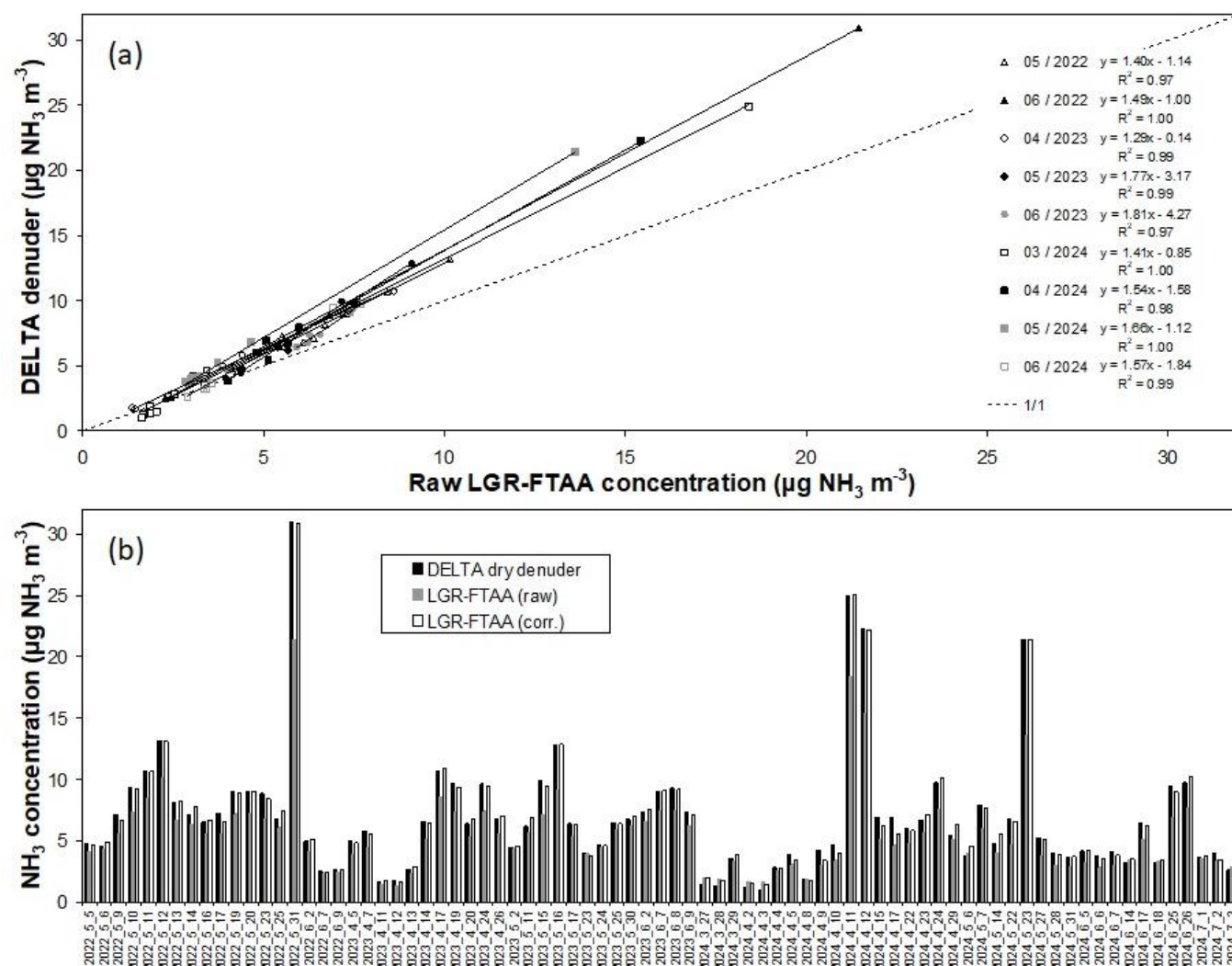
Figure 2: A posteriori correction procedure for LGR-FTAA QCL NH₃ concentrations using DELTA® dry denuder concentrations as a reference. (a) Linear regression of time-integrated DELTA® concentrations versus LGR-FTAA
395 **average raw concentrations calculated over each of the DELTA® sampling intervals from 2022 to 2024 (co-located sampling at 1.1 m above ground). (b) Time series of mean NH₃ concentrations for all DELTA® sampling intervals, with raw LGR-FTAA QCL concentrations and corresponding values corrected based on the respective regression slopes and offsets from (a).**

400

3.2 Ammonia concentrations and vertical profiles

Over all four spring measurement campaigns, half-hourly mean NH₃ concentrations measured by the LGR-FTAA, and corrected by regression vs DELTA values (Fig. 2) ranged from 0.1 to 194 µg NH₃ m⁻³, with an arithmetic mean and median

of 7.2 and 5.9 µg NH_3 m^{-3} respectively at height z_{mean}. During grazing periods, peak concentrations reached 112 µg m^{-3},

405   primarily driven by cattle activity and excreta deposition on the measurement field.

The measured NH_3 concentrations exhibited high temporal and vertical variability with differences before and after management activities such as grazing and N fertilization, but also between day and night and as a function of wind direction, as NH_3 plumes from nearby farms and animal housing buildings passed over the site. Larger NH_3 concentrations observed at upper heights (≥1.1 m) frequently indicated dry deposition events, where atmospheric NH_3 was taken up by the surface (for

410   example vertical profile in Fig. 3a).   Fluxes in background conditions (well outside of grazing and fertilization events) were bidirectional, with alternating patterns of small NH_3 emissions (primarily during daytime) and dry deposition (mostly at night and during wet conditions) (see supplement Fig. S14).

However, during cattle grazing and shortly after mineral and organic fertilization, the largest concentrations were typically observed near the surface (0.1–0.5 m) compared to upper heights (1.1–2.1 m), forming a vertical concentration gradient

415   characteristic of net NH_3 emission (Fig. 3b), where NH_3 released from the surface accumulates at ground level before being mixed upwards by turbulence. Figure 3c illustrates 2 weeks with contrasting 5-height NH_3 vertical concentration profiles, with the resulting AGM-derived fluxes, based on the top three heights, shown in Fig. 3d.
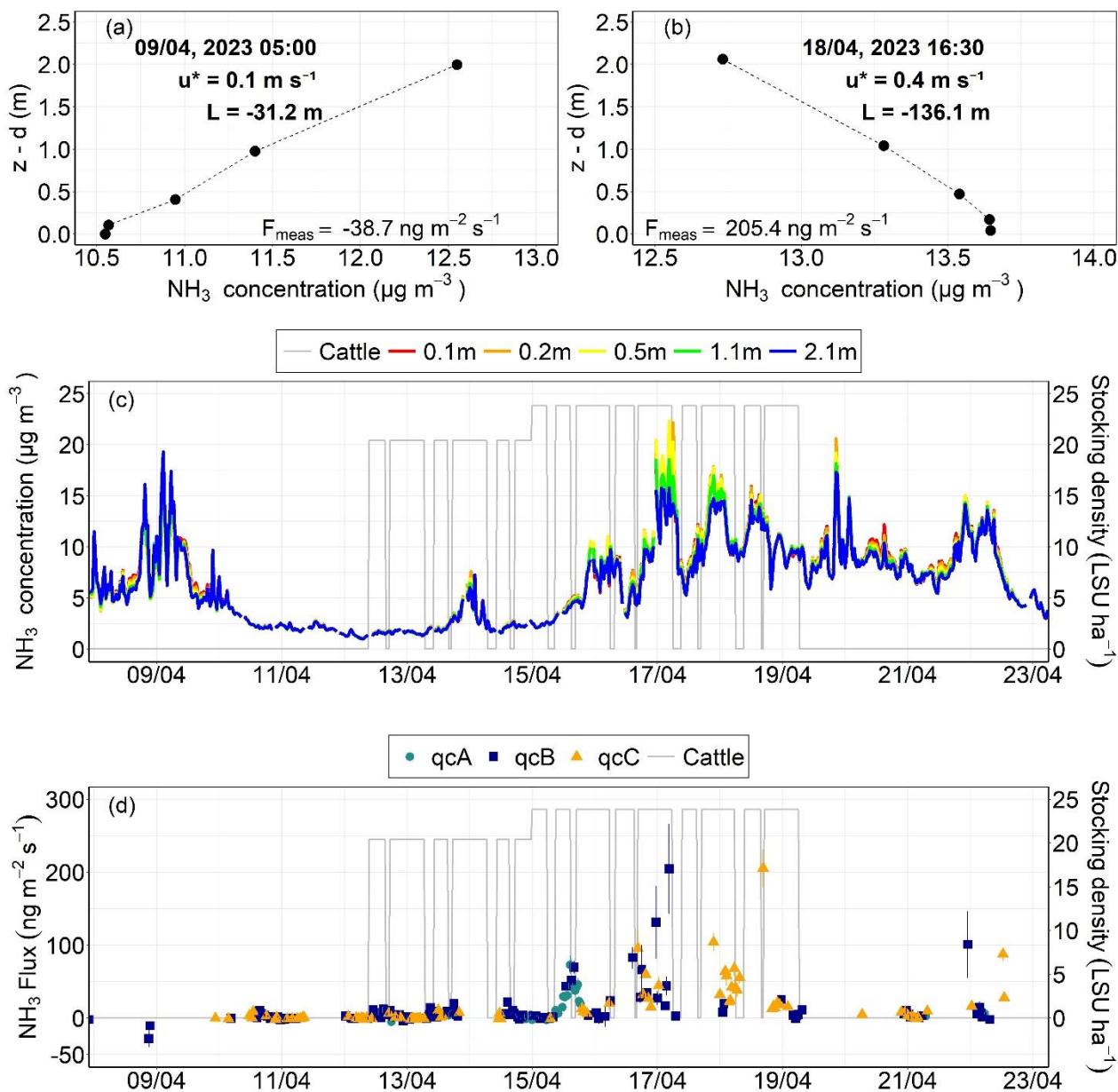
Figure 3: (a) Example of a vertical NH₃ concentration profile indicating dry deposition in background conditions (09/04, 2023, 05:00). (b) Example of an NH₃ concentration profile during grazing (18/04, 2023, 16:30), showing an emission event during windy neutral conditions. (c) Time series of NH₃ concentrations at different heights (0.1–2.1 m) illustrating the contrast between pre-grazing and grazing period. (d) Time series of NH₃ fluxes calculated by AGM over the same interval, positive fluxes indicate emission and negative fluxes indicate deposition.

3.3 Temporal variations of NH₃ fluxes in relation to grazing

430   Over the entire measurement campaign (springs 2021 to 2024), NH_3 fluxes were extremely variable across management activities (background or no management, grazing, fertilization), ranging from -626 (deposition) to +10235 (emission) ng m^{-2} s^{-1} (see Supplement Fig. S1-S4 for all fluxes measured on plot A). Although the largest NH_3 flux was observed after slurry application, this study focuses on grazing-induced emissions, which showed more persistent patterns compared to the short-lived peaks that followed fertilization. The ten cattle grazing events, for which sufficient flux data were available to describe

435   temporal patterns and investigate controlling factors, are summarized in Table 2 and shown in Fig. 4.

Fluxes measured during and shortly after grazing ranged from -113 to 3205 ng NH_3 m^{-2} s^{-1}, with the largest flux recorded during G9 (2024). Across the ten grazing events (Table 2), NH_3 emissions followed distinct temporal patterns, with larger emissions during daytime than at night (Fig. 5), and often but not systematically peaking toward the end of the grazing phase, before gradually returning to background levels within a week or two after cattle departure (Fig. 4).

440   The largest half-hourly flux levels observed during each of the 10 grazing events varied between around 200 ng NH_3 m^{-2} s^{-1} (see G4, G5, G10 in Fig. 4) and 3000 ng NH_3 m^{-2} s^{-1} (G8, G9), with more common event-based peak levels around 500-1000 ng NH_3 m^{-2} s^{-1} (G1, G2, G3, G6, G7). Figure S5 (supplement) shows that fluxes that were validated from both micrometeorological and footprint viewpoints, for the grazed plot of interest (flux quality classes qcA, qcB, qcC), but shown without footprint correction in Fig. S5, were most of the time significantly larger than micrometeorologically valid fluxes that

445   failed the 2/3 footprint criteria, in other words, fluxes that could be fully or partly representative of background bi-directional exchange of the adjacent plots. Over the ten grazing events, around 75% of the measured fluxes were net emissions (during the first two weeks following the start of grazing). These reinforce the hypothesis that grazing is a primary driver of NH_3 emissions, significantly increasing fluxes compared to background conditions. Over the 10 grazing events, Fig. 4 and Table 2 show a roughly equal distribution of fluxes between the qcB and qcC classes ("good" and "modest" quality), but much fewer

450   occurrences of qcA ("best" quality) fluxes, though this also reflects the somewhat arbitrary nature of the thresholds chosen to attribute classes.

It is also apparent that for some grazing events (e.g., G2, G7, G8) the valid flux data capture was patchy, not necessarily due to instrument malfunction or unsuitable micrometeorological conditions, but often due to insufficient footprint contribution by the plot of interest (i.e. the wind was blowing from unsuitable directions). Such fluxes, indicated by grey crosses in Fig. S5,

455   may be fully representative of the adjacent plot (A or B, depending on which is the plot of interest), or a mixture of both plots, highlighting the difficulty of characterizing temporal flux patterns in rotational grazing with one single flux measurement setup located on the divide.

460

Table 2: Summary of management practices, environmental conditions, NH₃ fluxes and quality metrics across ten grazing events (G1–G10). Data include NH₃ fluxes (ng NH₃ m⁻² s⁻¹), stocking density during the grazing interval (LSU ha⁻¹), grazing duration (DG), effective grazing days (EGD, defined as stocking density multiplied by grazing duration), grass nitrogen content, aboveground biomass measured before grazing started, and meteorological variables (average temperature, wind speed, relative humidity, soil water content and vapour pressure deficit). Flux data quantity and quality are represented by counts of half-hourly qcA, qcB, and qcC flux values. The qc$_{\mu met}$ percentage indicates the proportion of valid half-hourly flux measurements meeting quality criteria (0 or 1). The percentage of final valid flux data equals % qc$_{\mu met}$ minus the additional fraction removed due to insufficient footprint contribution.

Period	G1	G2	G3	G4	G5	G6	G7	G8	G9	G10
Date	09/04 – 19/04/22	15/04 – 19/04/22	20/05 – 31/05/22	12/04 – 28/04/23	19/04 – 28/04/23	11/05 – 25/05/23	25/05 – 10/06/23	10/04 – 25/04/24	15/05 – 30/05/24	20/06 – 04/07/24
plot	A	B	A	A	B	A	B	A	A	A
LSU ha⁻¹ (DG)	45(2.7)	44 (2.1)	55 (5.6)	23 (4.3)	24 (5.8)	33 (4.6)	30 (6.2)	29 (2.5)	16 (7.4)	17 (5.5)
EGD	122	93	237	127	138	150	185	72	118	94
Herbage N (%)	3.1	3.2	1.9	2.2	1.7	2.7	2.0	2.7	2.1	2.0
Biomass (t DM ha⁻¹)	3.8	3.6	5.6	5.3	4.7	5.7	5.6	4.5	6.5	5.1
Half-hour obs.	481	193	525	768	432	699	798	721	748	673
Mean NH₃ flux	129	208	121	13	29	45	67	93	250	14
Min. NH₃ flux	4	19	-12	-6	-4	-44	-28	-11	-8	-53
Med NH₃ flux	72	203	38	5	15	16	45	36	87	2
Max. NH₃ flux	801	385	1250	205	171	536	417	2682	3205	215
SE NH₃ flux	29	39	24	3	6	6	7	13	27	3
Rel. random error (%)	18	20	61	72	57	25	18	21	15	45
Air T (ºC)	12.1	13.1	14.5	10.8	11.6	13.3	18.3	10.2	14.2	17.5
Soil T (ºC)	12.8	14.7	18.5	12.6	13.3	15.4	20.1	12.5	16.5	19.9
Cumulative rain (mm)	3.2	0.5	29.4	41.6	32	5.5	2	8.3	37.6	7.5
WS (ms⁻¹)	1.3	1.2	1.3	1.8	1.7	1.9	1.6	1.7	1.6	1.3
RH (%)	73	74	75	77	77	75	69	78	82	77
SWC (%)	30	27	19	35	34	30	17	32	32	23
VPD (hPa)	4.7	5.1	4.9	3.3	3.4	4.4	7.6	3.2	3.2	5.5
qc$_{\mu met}$ % (0,1)	62	79	83	82	82	85	85	69	67	55
qcA	31	0	10	66	47	89	12	51	41	102
qcB	88	24	82	126	80	198	45	193	135	119
qcC	43	10	170	81	42	185	56	131	102	92
Valid flux data (%)	35	18	50	37	39	68	14	52	37	47
Deposition fluxes (%)	0	0	8	17	11	24	13	15	2	36
Emission fluxes (%)	100	100	92	83	89	76	87	85	98	64
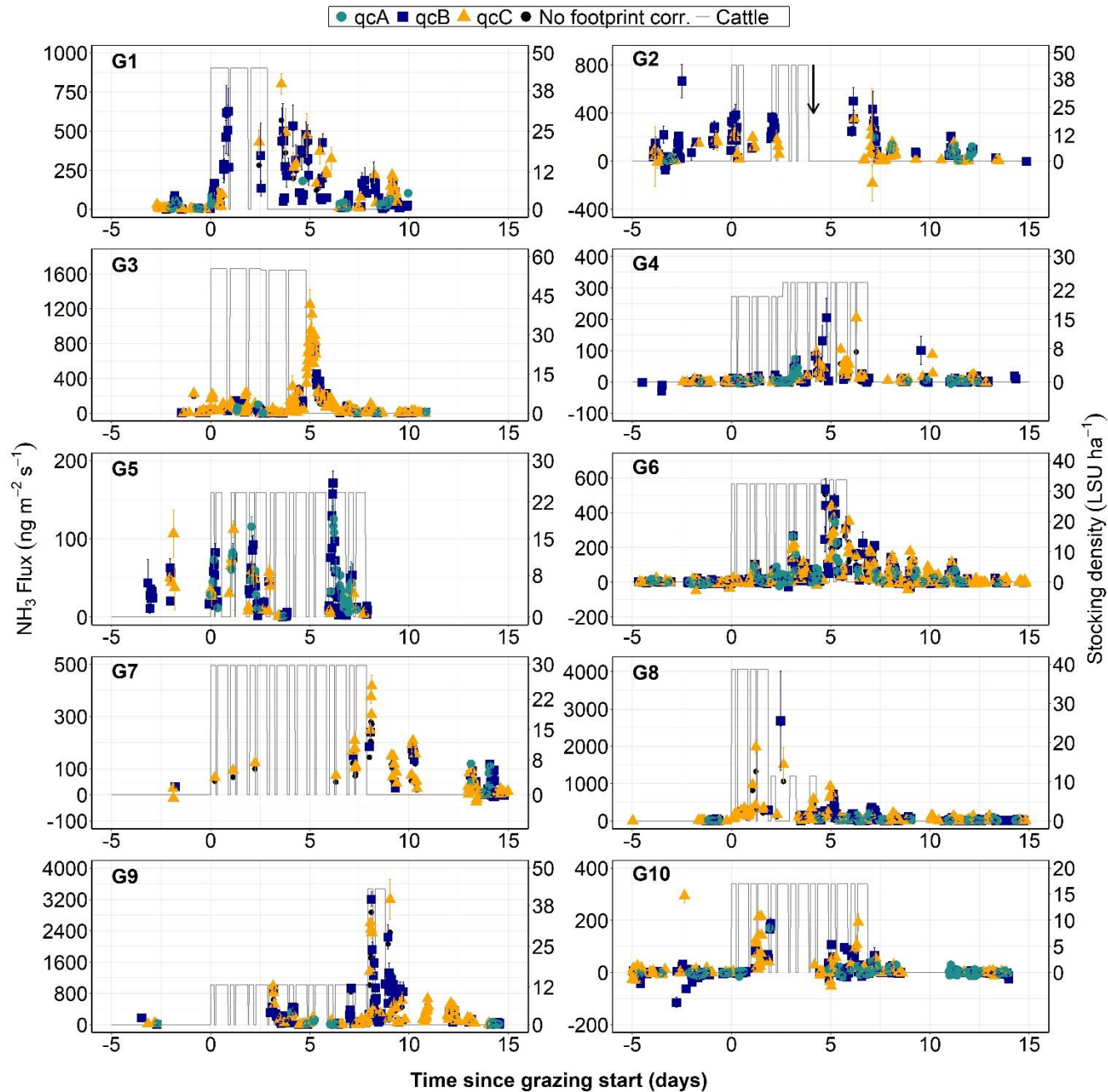
Figure 4: Temporal patterns of grazing-induced NH₃ fluxes (symbols) and stocking density (grey lines), measured up to 15 days after the onset of grazing for the 10 events summarized in Table 2. Coloured symbols (green circles, blue squares, orange triangles) show final corrected fluxes for the plot of interest in three quality classes (qcA, qcB, qcC, respectively, as defined in Table 1), with error bars showing random errors calculated from Eq. 10. For comparison, black circles indicate the same fluxes without footprint correction. The arrow in G2 indicates a fertilization application of 39 Kg NH₄NO₃-N ha⁻¹ that occurred just after grazing ended. Note that different y-axis scales are used due to variations in flux magnitude between grazing events.

470

475

3.4 Environmental controls on NH₃ fluxes

Apart from cattle slurry spreading, which triggered large but short-lived NH₃ emission pulses (see fluxes on 31/05/2022 in Fig. S2 in Supplement), the primary driver of NH₃ emissions on the pasture was the presence of grazing animals on the field. Measurement of ammonium and nitrate content in the topsoil samples in different strata from 0-30cm depth showed a clear enhancement of mineral N as a result of grazing during the 2023 and 2024 seasons (Fig. 6). But, as shown in Fig. 4, the observed emissions did not occur systematically when animals were present, nor did the peak fluxes in each event scale with the stocking density during the grazing phase. Thus, apart from the supply of labile N to the soil through animal excreta, which can be assumed in first approximation to scale with stocking density multiplied by grazing duration (effective grazing days or EGD in Table 2), other environmental control factors must be invoked to explain the observed dynamics within each grazing event, and the differences between the ten grazing events.

Clear differences in fluxes between day and night hint strongly at control factors that vary diurnally, i.e., primarily meteorology. Since animals grazed on the field both day and night, apart from 2 hours early morning and evening in the milking parlour, animal presence can be ruled out as the driver of day-night differences. The distinct diurnal cycle in NH₃ emissions in most of the ten grazing events is shown in Fig. 5, with fluxes peaking in the afternoon (12:00–16:00) and declining overnight (0:00–6:00).

Meteorological variables with marked diurnal patterns include air (and soil) temperature, relative humidity, VPD, global and net radiation, wind speed, and also atmospheric turbulence (u∗) and stability/instability (L), all known to influence the surface-atmosphere exchange of NH₃ (Flechard et al., 2013). Following standard thermodynamics of the equilibrium between aqueous-phase NH₄⁺ and gas-phase NH₃, lower nighttime fluxes are consistent with reduced volatilisation under cooler conditions and higher relative humidity. Correlation analysis indicated that several meteorological variables were significantly correlated with NH₃ fluxes (Tables S2 and S3 in the Supplement). Vapour pressure deficit and relative humidity indeed frequently showed a significant correlation ($p < 0.01$) with NH₃ fluxes, especially during periods such as G4 and G6 (Fig. 7), but this pattern was not isolated to VPD and RH alone. Temperature (air and soil), wind speed, and friction velocity also exhibited significant positive correlations ($p < 0.01$) across several grazing events (see Fig., S6-S8 in supplement).

Moreover, the aforementioned potential (micro-)meteorological drivers are often intercorrelated, positively or negatively on a diurnal basis: higher temperatures typically occur in the daytime at the same time as high VPD, low RH, unstable atmospheric conditions and large friction velocity (and vice-versa at night). Therefore, this multi-collinearity implies that NH₃ emissions are modulated by the combined influence of several meteorological factors rather than a single dominant driver.

By contrast, soil moisture does not exhibit a systematic diurnal cycle but responds to rainfall and evapotranspiration over longer time scales (days to weeks). Precipitation events appeared to reduce emissions in particular during some grazing periods (e.g., G4), possibly by increasing surface wetness and physically limiting NH₃ volatilisation by reducing soil pore diffusivity,

but also possibly because rainfall often coincided with cooler conditions and lower VPD. Conversely, the largest grazing-related NH_3 fluxes in spring 2022 (peak on 25/05/2022, phase G3) occurred one day after the end of a cumulative rainfall episode of 30 mm (Fig. S2 in Supplement), which may have triggered a large emission response.

515
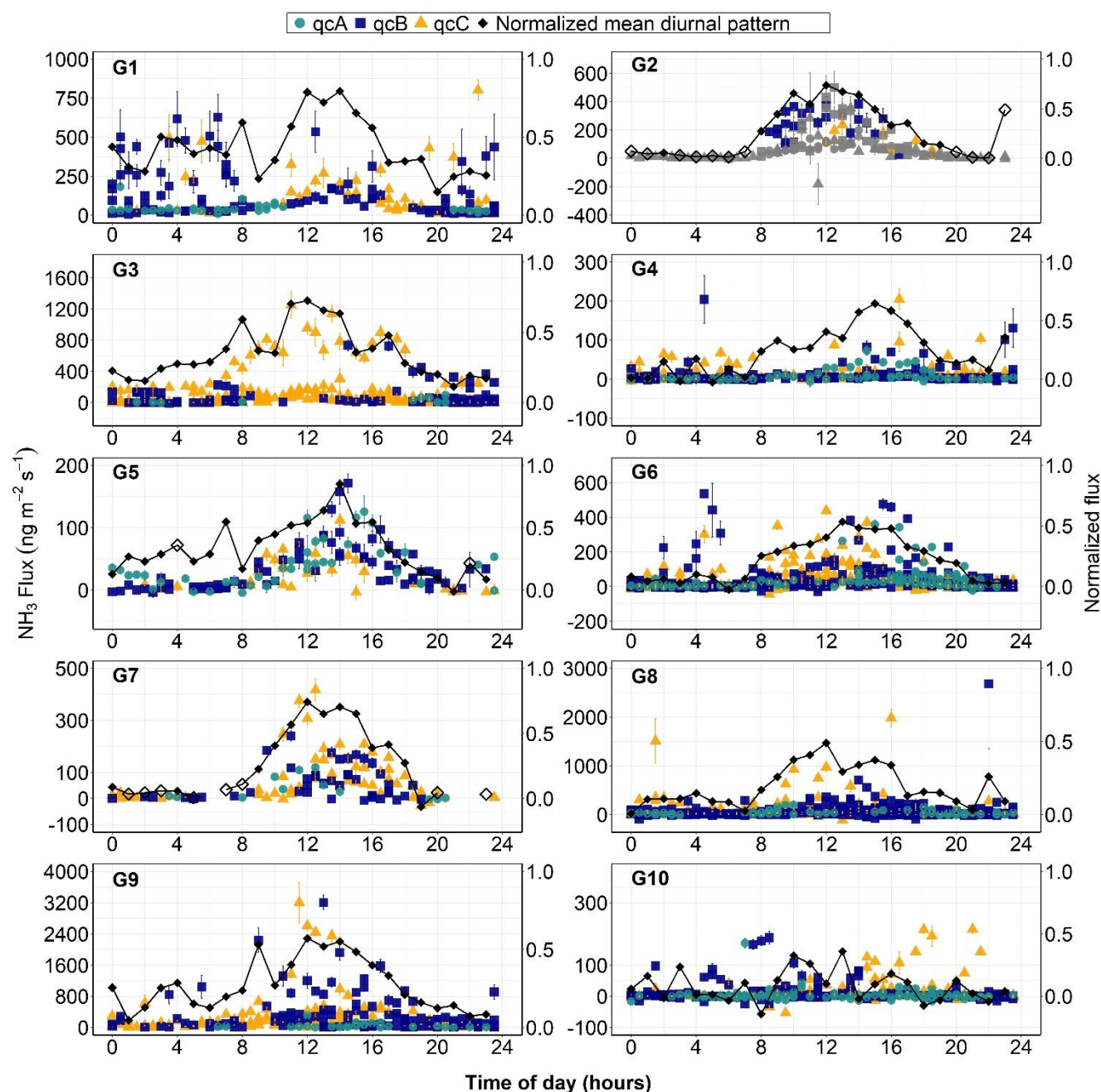
Figure 5: Diurnal variations of NH₃ fluxes for the 10 grazing events summarized in Table 2. Coloured symbols (green circles, blue squares, orange triangles) show final corrected fluxes in three quality classes (qcA, qcB, qcC, respectively), with error bars showing random errors calculated from Eq. 10. The black line shows the mean normalized diurnal flux pattern calculated using the DVmax method (Eq. 12, see also Fig. S10 in supplement). Black diamonds indicate hourly averages based on more than three data points; unfilled diamonds represent averages based on fewer than three. Fluxes measured after the mineral fertilization event in G2 are shown in grey. Note that different y-axis scales are used due to variations in flux magnitude between grazing events.

525
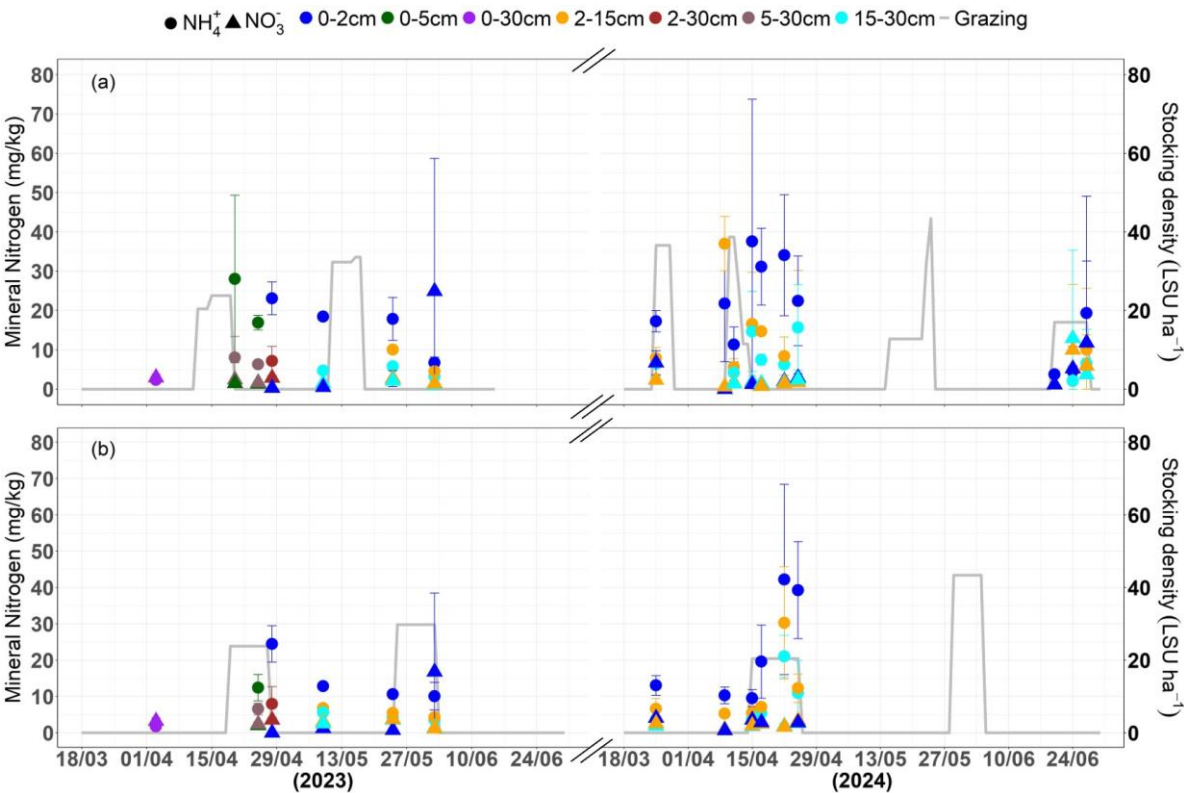
Figure 6: Soil mineral nitrogen concentrations (NH₄⁺ and NO₃⁻) variation across different soil depths (0–30 cm) in relation to grazing activity in 2023 and 2024 for (a) Plot A and (b) Plot B. Error bars denote standard deviations across replicates.

530
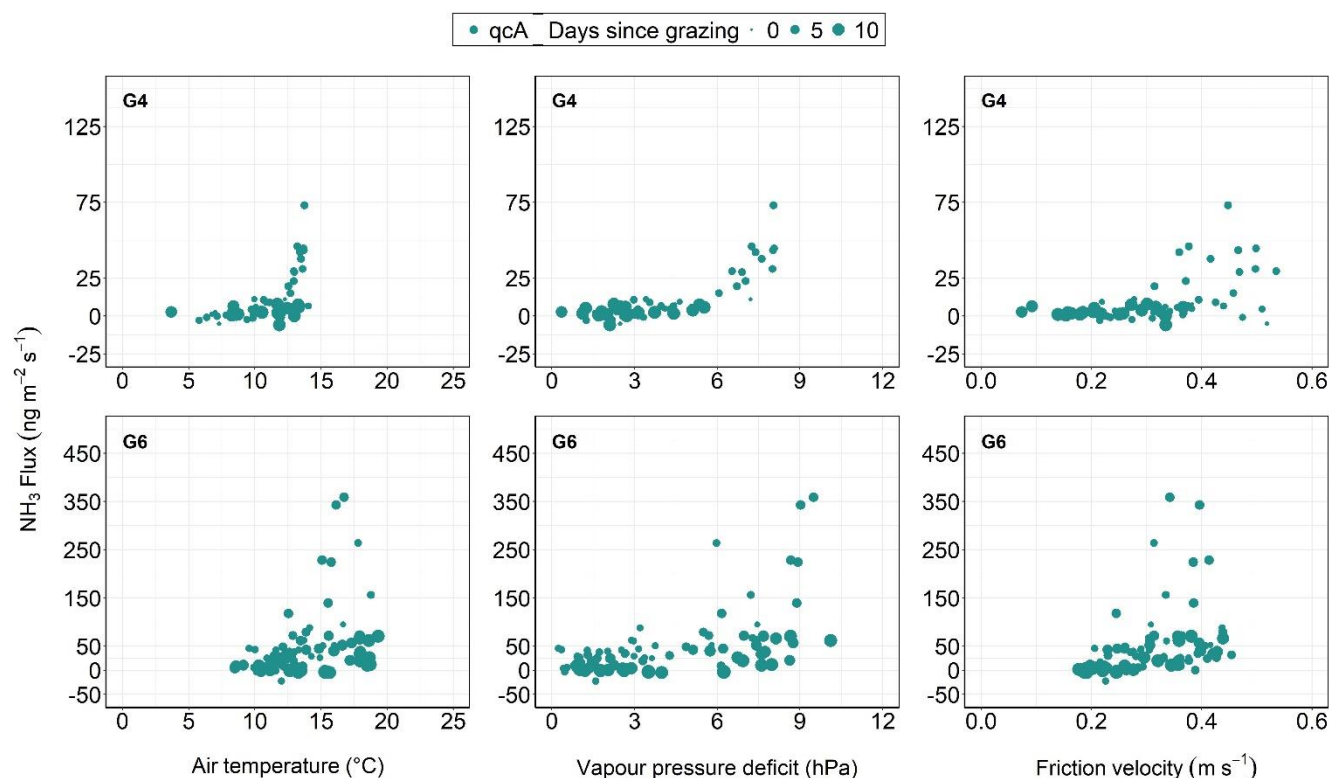
Figure 7: Relationship between NH₃ fluxes and air temperature (left), vapour pressure deficit (middle) and friction velocity (right), for grazing events G4 and G6. Half-hourly qcA fluxes are shown, represented by green circles. Symbol sizes correspond to the time elapsed since grazing started. Note: Different y-axis scales due to variations in flux magnitude between grazing events.

3.5 Uncertainties in measured fluxes

Fluxes classified as qcA accounted for 16%, while qcB made up 46%, and qcC contributed 38% of all valid fluxes (Table 2). The mean relative random error in AGM NH₃ fluxes across the ten grazing events ranged from 15% to 72%, with a mean overall value of 35%, with u_* contributions to total random uncertainty ranging from 17% to 64%, while the error in the stability-corrected NH₃ gradient was larger, contributing from 36% to 83% (Table S1 in supplement).

Systematic errors in AGM-derived fluxes are more difficult to quantify. Storage change errors were small (median relative error 1.4%; rel. error smaller than 10% (20%) in 82% (89%) of cases). However, no flux data for chemically-interacting pollutants was available to quantify gas-particle-inter-conversion (e.g., reaction of NH₃ with HNO₃ to form NH₄NO₃ aerosol or evaporation of volatile NH₄⁺ aerosol); this effect was assumed to be small at this rural agricultural site, where NH₃ concentration was much larger than chemically interacting acids (the mean molar ratio of NH₃ to the sum of strong acids

[HNO$_3$+SO$_2$+HCL] measured by DELTA® was 11.2). By contrast, horizontal advection was likely a larger source of systematic error. Two effects may be distinguished; i) advection of NH$_3$ plumes from local farms and animal housing buildings, the local dairy farm being located approximately 300-400 m to 120°-140° SE, which however was not a dominant wind

550   direction during the study (Fig. 1); and ii) differential footprints of the different measurement heights in the vertical concentration profile, and their location in relation to the finite-sized field.

One way to assess the potential influence of advection and concentration footprint issues over the field is to calculate AGM fluxes using different measurement height ranges to compute Eq. (3). As shown in Figure 8, there were systematic biases in fluxes computed from different height ranges, compared with the default flux estimates that used the range 0.5-2.1 m. Fluxes

555   estimated from the full profile down to the lowest height (0.1–2.1 m) were consistently lower, with regression slopes of 0.22–0.27, indicating a 73-78% underestimation. With the lowest height excluded (range 0.2–2.1 m), the underestimation was less pronounced, with regression slopes of 0.59-0.66 (34-41% lower than default). Fluxes derived from the upper two heights only (range 1.1–2.1 m) were 30% larger than the default estimate if the whole dataset was considered (including the few very large slurry spreading-induced emissions); however, for lower flux magnitudes (<2000 ng m^{-2} s^{-1}), as typically observed during

560   grazing, this height-dependent bias was much reduced to approximately 7%.

565
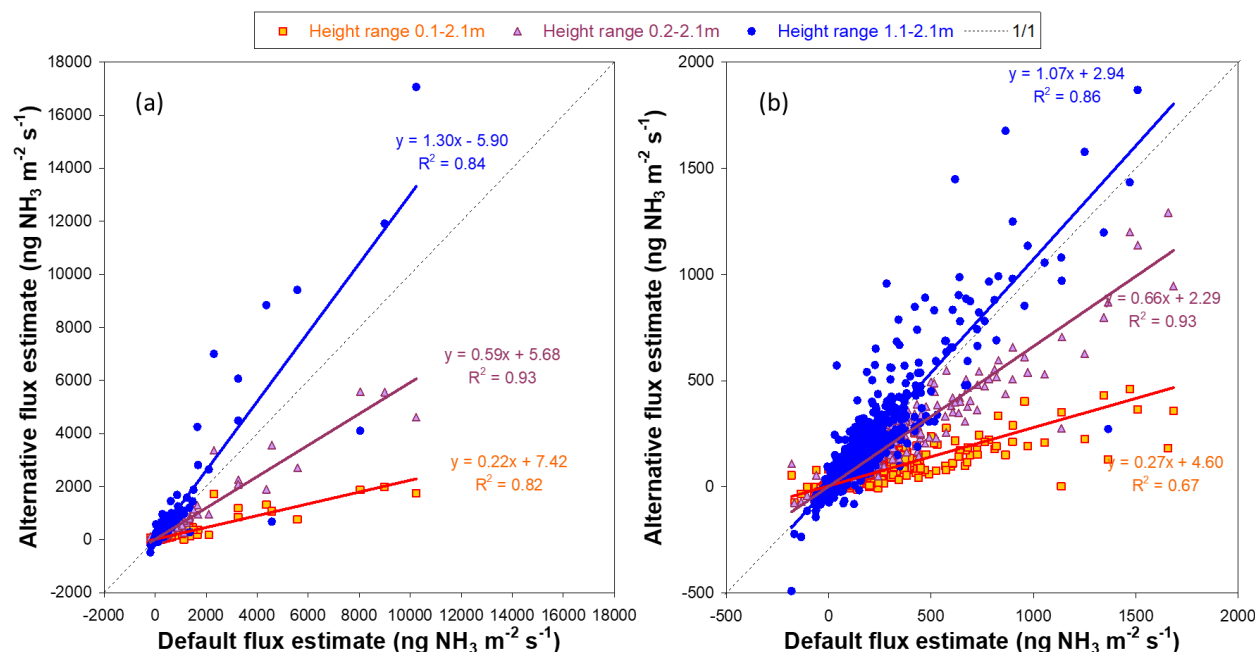
Figure 8: Sensitivity of NH₃ flux estimates to measurement height selection for (a) the whole flux dataset including slurry spreading events and (b) fluxes only up to 2000 ng m⁻² s⁻¹ (more characteristic of grazing-induced emissions). Default fluxes (x-axis) are based on the default height range used for flux calculation (0.5–2.1 m), while alternative fluxes (y-axis) are calculated using 0.1–2.1 m (orange squares), 0.2–2.1 m (purple triangles), and 1.1–2.1 m (blue circles). Regression lines illustrate deviations from the 1:1 line (dashed), highlighting strong underestimation if the lowest measurement heights were included.

3.6 Grazing event-based cumulative fluxes and emission factors

Given that emissions typically returned to baseline within 15 days, cumulative flux estimates were calculated over this interval (Table 3), based on available flux data and the gap-filling procedure using the mean diurnal patterns described in Sect. 2.6. Cumulative NH₃ emissions over 15-day periods ranged from 105 to 2190 g N ha⁻¹ using the DVmax method and 160 to 2322 g N ha⁻¹ using the DVavg method. Cattle head-based EF values showed substantial variability, ranging from 1 to 21 g NH₃-N cow⁻¹ grazing d⁻¹ for DVmax and 1 to 23 g NH₃-N cow⁻¹ grazing d⁻¹ for DVavg. Similarly, the EFs based on the fraction of deposited N emitted as NH₃ ranged from 1-18% and 1-20% for DVmax and DVavg respectively. The highest EF (for both approaches) was recorded in the G8 campaign (2024). The complete time series of gap-filled NH₃ fluxes for the whole dataset are shown in Fig. S11-S12 in Supplement).

Table 3: Cumulative NH₃ emissions (g N ha⁻¹) and emission factors (per livestock unit and fraction of the excreted N) for eight grazing events. Cumulative fluxes were calculated using the DVmax and DVavg gap-filling methods based on mean diurnal variation (see Methods). Grazing events G2 and G7 were excluded from cumulative and EF estimation due to low data availability.

Period	Cumulative fluxes		Urinary N excreted		EF per LSU		EF relative to urinary N	
	DVmax	DVavg	Total herd	Per cow	DVmax	DVavg	DVmax	DVavg
	(g N ha⁻¹)		(Kg N ha⁻¹)	(g N LSU⁻¹)	(g NH₃-N cow⁻¹ grazing d⁻¹)		(%)	
G1	1149	1637	11.5	94	9.4	13.4	10.0	14.2
G3	699	702	15.2	64	2.9	3.0	4.6	4.6
G4	174	179	13.9	109	1.4	1.4	1.3	1.3
G5	150	160	11.8	86	1.1	1.2	1.3	1.4
G6	411	438	13.3	89	2.7	2.9	3.1	3.3
G8	1482	1674	8.3	115	20.6	23.3	17.9	20.2
G9	2190	2322	14.5	123	18.5	19.6	15.1	16.0
G10	105	206	5.9	63	1.1	2.2	1.8	3.5

590

4 Discussion

4.1 Methodological uncertainties and limitations in AGM flux measurements

4.1.1 Systematic versus random errors in AGM flux measurements

Evaluating measurement quality is crucial for ensuring confidence in the collected observations (Csavina et al., 2017). Flux
595 measurements are subject to both random and systematic errors, influenced by instrument limitations, methodological assumptions, and environmental variability (Brümmer et al., 2022). Standard random error analysis likely reflects the smaller fraction of the overall uncertainty. Systematic errors associated with the AGM have been discussed in previous papers (Fowler and Duyzer, 1989; Sutton and Fowler, 1992; Loubet et al., 2013), and are likely substantially larger, though much more difficult to quantify. Some systematic errors are related to measurement conditions that invalidate the universal assumption that the
600 vertical flux is constant with height; namely, chemical production or consumption of NH₃ between the measurement height and the surface, storage changes in the air column (Eq. 7), and horizontal advection. Some systematic errors stem from unfulfilled assumptions in flux-gradient relationships

4.1.2 Effects of the NH₃ sampling line

605 Ammonia is a notoriously difficult gas to sample and analyze (Ellis et al., 2010). In this study, standard calculations of the relative error from random sources (Eq. 10-11), provided average values in the range 15–72% of the absolute flux, based on

turbulence sampling limitations and dispersion in NH_3 concentration gradient slopes. However, AGM requires accurate concentration gradient measurements, and NH_3 adsorption onto sampling tubes and instrument surfaces very likely produced smoothing of high-frequency concentration changes and carry-over of NH_3 from one sampling height to the next. This effect
610 likely occurred despite a large sampling flow rate and a single, heated and insulated sampling line used to minimize condensation and accumulation/loss effects. Such processes always result in an underestimation of vertical gradients, whether positive or negative; but the gradient (flux) underestimation was likely more pronounced during night and any other cool, humid conditions, than during dry daytime conditions. The observed diurnal cycles in fluxes during grazing events (Fig. 5) may for this reason be exaggerated; emissions may have in reality been larger at night than the data suggest. On the other hand,
615 the measurement system was often able to detect deposition gradients in background conditions, even during night-time cool and high humidity conditions (e.g., Fig. 2a). Overall, no objective criteria (e.g., comparison to another independent flux measurement system) was available to us to quantify the magnitude of the NH_3 "stickiness" effect.

4.1.3 Fundamental assumptions in AGM

620 A key source of uncertainty in this study involved the determination of a suitable concentration measurement height range, within the whole vertical profile (0.1 – 2.1 m) of the mast lift system, that could be considered at equilibrium with the upwind footprint within the pasture field. Low measurement heights on the mast are highly influenced by the near field, while upper heights look further upwind; a standard requirement in AGM is a homogeneous upwind fetch up to a certain distance, i.e. that the near field and far field have similar characteristics for soil, vegetation, roughness, etc. Fluxes computed using
625 measurements including and above 0.5 m were adopted in our study as the best estimate because the lower two heights (0.1 and 0.2 m) were considered to be footprint-influenced by the ungrazed area within the enclosure surrounding the flux tower and ancillary equipment. This hypothesis was consistent with vertical profile observations such as Fig. 3b, often showing a deviation of the two lowest heights from the assumed log-linear profile development within the inertial sublayer. Furthermore, the exclusion of the lower height (0.1-0.2m) from the vertical gradient slope calculation was consistent with the AGM
630 requirement that vertical profiles should be measured in the inertial sublayer, well above the roughness sublayer (RSL). The Monin-Obukhov similarity theory is considered applicable only above the RSL (Högström, 1996). Given that the RSL depth is estimated to be 1.5-2.5 times the canopy height (Melman et al., 2024), and a typical grass height of 0.1-0.2 m in our study, the lowest 40-50 cm of the profile should be (and were) excluded from flux calculations.

For technical reasons the 0.5 m measurement height was no longer available for flux calculations from May 2023 onwards,
635 reducing the available profile heights to 1.1 m and 2.1 m (Sect. 3.5). However, the reasonable agreement for moderately large fluxes (up to 2000 ng m^{-2} s^{-1}; slope 1.07, Fig. 8b) between the default height range (0.5 – 2.1 m) and the upper two heights only (1.1 – 2.1 m) supported the hypothesis that potential horizontal gradients and differential concentration footprints did not greatly bias fluxes, despite the relatively small field size and upwind fetch (100-150 m for the main wind SW and NNW directions, see Fig. 1).

640 Nevertheless, spatial heterogeneity arising from uneven grazing, rumination and urination behaviours likely resulted in localized concentrated urine deposition (N hotspots) within the pasture. When located upwind of the flux measurement tower, such hotspots would invalidate the assumption of near-field/far-field homogeneity, and depending on whether the hotspots were close to the tower, or further upwind, the resulting emission gradient would have been over-estimated or under-estimated. Whatever the case may be, the heterogeneous distribution of deposited urine-N inherent in grazed grasslands was certainly an

645 important factor in increasing the uncertainties associated with AGM-derived estimations.

The classical AGM assumes that eddy diffusivities for momentum (K_M) and scalars (K_H) are equal under neutral and stable conditions (Thom, 1975), but this assumption has been challenged in more recent studies (Flesch et al., 2002; Stull, 2012; Wilson, 2013; Foken, 2006). Further, the stability corrections, derived for vertical scalar profiles derived in the 1960s-1970s (e.g., Dyer and Hicks, 1970), have been re-evaluated in several publications (e.g., Högström, 1988; Foken, 2006). They were

650 found to be acceptable within the margin of instrumental error for moderately unstable conditions, but more questionable for stable conditions and very unstable conditions, although no universal consensus has yet been found (Högström, 1996). Such uncertainties imply that traditional AGM methods could be biased with respect to flux calculations (Anderson et al., 2019). Although this study retains the original AGM assumptions and stability correction functions from the 1970s, we recognize that potential deviations may have introduced additional uncertainty in our flux estimates.

655 **4.1.4 Footprint-derived corrections of measured fluxes**

Flux correction procedure based on footprint modelling and attribution (Sect. 2.4.5) introduced further uncertainty related to the accuracy of the spatial extent of footprint, and resistance parameterizations used in the estimation of background fluxes (Eq. 8-9 and supplement Fig. S14). A comparison of flux estimates by AGM and bLS inversion of the concentration increment over the field indicates that AGM can underestimate NH_3 emissions by up to 9% without footprint correction (Kamp et al.,

660 2021). Sintermann et al. (2012) recommended considering that at least half of the flux footprint must originate from a given field for accurate flux assessment. We used a more severe threshold of two-thirds for each half-hourly flux footprint to originate from the relevant field. The resistance-based flux model used in this study to simulate background exchange was meant to address the potential emission underestimation from incomplete flux footprint coverage, but model resistance parameterizations come with significant uncertainties of their own. A combined approach integrating AGM measurements

665 with other independent flux measurement methods (EC, BLS inversion, etc) could improve NH_3 flux assessments in future studies.

4.2 Ammonia exchange dynamics in relation to grazing-soil-ecosystem interactions

The magnitude of NH_3 emissions has been shown to be controlled by environmental and management factors reflecting the interplay of dairy and grazing management, nitrogen distribution, and atmospheric conditions (Jarvis et al., 1991). During

670 grazing, NH_3 fluxes exhibited a characteristic gradual increment, often peaking either toward the end or shortly after cattle

departure, before declining within a week. This pattern observed across multiple grazing events, aligns with previous studies (Bell et al., 2017; Jarvis, et al., 1989b; Laubach et al., 2013; Voglmeier et al., 2018), highlighting how the combined effects of excreta deposition (labile N addition to soil), vegetation disturbance, and atmospheric conditions (weather and turbulence) interact to shape NH_3 emission dynamics.

675 The dominant driver of NH_3 emissions during grazing is considered to be urine deposition, which introduces large amounts of nitrogen as urea in concentrated patches, especially in the uppermost horizon (e.g., 0-2cm in Fig. 6). Another effect of urine deposition is alkalinity enhancement. Urea hydrolysis drives ammoniacal nitrogen formation from the deposited N and promotes gas-phase NH_3 release (Giltrap et al., 2017; Laubach et al., 2013; Selbie et al., 2015). Apart from meteorology, the extent of NH_3 release is strongly influenced by several intrinsic ecosystem factors including soil pH and cation exchange

680 capacity. In this study, late winter pre-season pH values were in the range of 5.5-6, but values measured during or after grazing often reached 6.5-7 (Fig. S9 in Supplement). In addition, herbage nitrogen content affects the nitrogen composition of excreta (Jarvis et al., 1989a; Jarvis et al., 1989b). In this study, high herbage N in G1 (3.1%, see Table 2) coincided with large volatilisation from deposited urine, which may indicate the role of excreta quality in driving emissions, although this is difficult to confirm given other confounding factors such as meteorology.

685 The interaction between vegetation and soil NH_3 emissions further modulates fluxes. Before grazing, dense canopies absorb atmospheric NH_3 through stomatal uptake and non-stomatal deposition (Asman et al., 1998; Flechard et. al., 2013; Harper et al., 1983). However, grazing disrupts the balance by reducing biomass, shortening canopy height, and decreasing leaf surface area available for NH_3 recapture, leading to increased net emissions. This effect was particularly evident in G1, G4, and G6 where peak fluxes coincided with cattle departure when the canopy was most reduced (Fig. S2c-S3c). The removal of taller

690 vegetation increases wind penetration into the canopy and re-couples the atmosphere with the soil surface, facilitating rapid vertical NH_3 transfer (Denmead et al., 1976). After cattle removal, plant regrowth resumes, restoring foliar surfaces for NH_3 exchange and gradually reducing soil emissions by the double effect of root N uptake and canopy recapture of soil-emitted NH_3.

Nonetheless, post-grazing fertilization raises the N status of the system and the stomatal compensation point (Loubet et al.,

695 2002), promoting potential NH_3 emission by leaves; bi-directional exchange including small net ecosystem emissions (up to ~ +50 ng m^{-2} s^{-1}) were frequently observed at our site in background conditions, even after several weeks following the latest grazing or fertilization event (see e.g., Fig. S1, S14 in Supplement). Soil nitrogen levels post-grazing are also influenced by competing soil microbial processes, including nitrification and denitrification, which further regulate NH_3 volatilisation (Selbie et al., 2015).

700 Cattle movements on the field play a role in regulating NH_3 dynamics through the spatial distribution of excreta. Exceptionally large NH_3 fluxes were observed in spring 2024 (with peaks exceeding 2000 ng m^{-2} s^{-1}) and may be partly explained by observations showing that cattle often aggregated near the water trough SSW upwind of the measurement system, leading to localized nitrogen hotspots, a well-documented driver of flux variability (Bell et al., 2017; Laubach et al., 2013). Such hotspots may have intensified NH_3 emissions in some parts of the flux footprint, an effect also observed for greenhouse gas emissions

705 in concentrated excreta zones (Mitchell et al., 2021). In G8, such an aggregation effect would be consistent with the large spatial variability in topsoil NH_4^+ observed post-grazing (Fig. 6a), indicating localized N accumulation in some parts of the field. This may suggest that uneven nitrogen distribution contributed to some of these peaks, but only if flux footprint areas coincided with N hotspots, which could not be verified experimentally. In addition, some of the very large emission fluxes observed during G8 were measured at night, in conditions of very low turbulence ($u* < 0.05$ m s^{-1}) associated with very large

710 vertical emission gradients (tens of µg NH_3 m^{-3} difference between measurement heights). Although they passed all criteria in the flux selection procedure (see Sect. 2.4.4), the uncertainty in such fluxes is very large, with many data points assigned qcC (modest quality), and as such they should not be over-interpreted.

Soil compaction from trampling on such hotspots may have influenced emissions by reducing infiltration, leading to longer retention of urine on the surface (Luo et al., 2017), and prolonged NH_3 volatilisation properties. The introduction of a second

715 cattle group in G9 (43 LSU ha^{-1} after seven days of initial grazing at 13 LSU ha^{-1}) likely enhanced N deposition, contributing to the strong increase in observed emissions. Reducing localized emissions may require targeted management strategies. Increasing the number of water trough placements could minimize aggregation areas, while Bell et al. (2017) suggest that smaller paddocks with increased grazing densities may help distribute nitrogen more uniformly and mitigate NH_3 emission hotspots.

720

4.3 Effect of meteorology

Previous studies have highlighted the challenge of linking NH_3 fluxes directly to meteorology due to the strong interdependence of environmental variables (Jarvis et al., 1991). In this study, temperature, relative humidity, vapour pressure deficit (VPD), wind speed and turbulence (u_*) were all strongly correlated with NH_3 fluxes (Table S2), but cross-correlations

725 on a diurnal basis between these variables make it difficult to isolate single effects, especially since a further temporal dimension should be added to characterize the dynamics of soil nitrogen and vegetation LAI and canopy height in response to grazing over 1-2 weeks.

Temperature influences NH_3 volatilisation directly by modulating substrate availability in the urine patch through urease activity, and by controlling the aqueous/gaseous phase partitioning of ammoniacal nitrogen (Reynolds and Wolf, 1987). It also

730 has indirect effects through elevated VPD, which accelerates soil surface evaporation and plant transpiration, also forcing NH_x out of the aqueous phase at the soil–plant–atmosphere interface. This effect was particularly evident in G4 and G6, where high VPD levels coincided with peak emissions (Fig. 7). Conversely, low VPD conditions (or high relative humidity) are associated in the literature with enhanced deposition onto plant and soil surfaces promoting non-stomatal NH_3 uptake surfaces and further suppressing net volatilisation to the atmosphere (Bell et al., 2017; Flechard et al., 2013; Freney et al., 1983), which appears to

735 be consistent with the observed flux patterns. Cooler night-time temperatures also slow urea hydrolysis.

Nevertheless, several nighttime data points exhibited relatively high NH_3 gradients, which despite low friction velocity, yield

high emissions calculated from the flux-gradient equation. In such intermittent turbulence conditions, the uncertainty in the AGM flux is very large and these data can be treated as outliers, but the data nonetheless suggest that under stable night conditions, NH_3 may accumulate near the surface during temperature inversions, trapping emissions closer to the ground due
740 to reduced atmospheric mixing and limited vertical NH_3 transport. When minimal turbulence resumes, this accumulated NH_3 may be transported and released resulting in spikes that might not represent instantaneous emission processes but rather delayed transport of previously emitted NH_3. These exceptions indicate that while fluxes increase with VPD under turbulent daytime conditions, specific micrometeorological conditions may also elevate nighttime emissions.

Rainfall events have a dual impact on NH_3 fluxes. Generally, precipitation may reduce emissions by diluting urea from urine
745 patches, lowering NH_4^+ concentrations at the soil surface and enhancing infiltration (Harper et al., 1983; Walker et al., 2013). These effects were observed in G4, where persistent rainfall and soil moisture dampened NH_3 emissions. However, light rainfall events may temporarily increase NH_3 emissions by dissolving surface nitrogen, facilitating microbial activity, and increasing substrate availability (Sommer et al., 2004). Overall, warmer conditions corresponded with increased emissions (G6) whereas cooler, wetter periods (e.g., G4) exhibited comparatively lower NH_3 fluxes.

750

4.4 Variability in emission factors in this and other studies

Grazing-induced NH_3 fluxes in this study persisted for several days and, in cumulative terms, were larger than those observed following NH_4NO_3-N fertilizer applications (Fig. S2–S4). The estimated nitrogen input from grazing events (6–15 kg N ha^{-1})
755 was lower than that from mineral fertilization (25–39 kg N ha^{-1}), however cumulative NH_3 emissions were often higher under grazing. This highlights the significance of grazing as a field-scale NH_3 source. While grazing is often considered a mitigation strategy relative to CAFOs, our findings underscore that grazing with its high volatilisation potential from urine patches is still a critical ecological contributor to NH_3 emissions under field conditions. The cattle head-based EF values we derived for eight grazing events at our site exhibited a very large variability (factor of ~1 to 23) but with a majority (five out of eight) EF values
760 of the order of 1-3 g NH_3-N cow^{-1} grazing d^{-1}. Since only eight EF values could be derived from our dataset (Table 3), and since the number of potential explanatory macro-drivers was almost as large (mean event-based values of soil/air temperature, VPD or RH, wind speed or u_*, rainfall, cattle diet or herbage N content), no statistical multivariate analysis could be applied to derive the share of EF variance explained by individual variables. This would be all the more difficult due to cross-correlations between meteorological drivers.
765 In 2024, NH_3 EF peaked at 19–23 g NH_3-N cow^{-1} grazing d^{-1} during G8-G9, but the available data do not offer any obvious explanation for these large values. Most of the EF estimated at our site fell within the range of other studies (Table 4), in which the largest values of 53.9 g NH_3-N cow^{-1} grazing d^{-1} were measured in conditions of very large stocking density (Laubach et al., 2013). However, the variability observed in grazing-induced emissions remains relatively small compared to that reported from dairy buildings, where EFs can range from 0.7 to 205.9 g NH_3-N cow^{-1} day^{-1} (Hristov et al., 2011).

770 Valid flux data capture at our site was on average around 40% (range 18-68%) across the ten grazing events, in large part due to footprint issues associated with the division of the field into two grazing paddocks, with the measurement setup in the centre. Thus gap-filling accounted for 60% of the time on average. It follows that the uncertainty in the cumulative fluxes and EF depends to a large extent on the accuracy of the gap-filling procedure. A normalized diurnal variation approach to fill data gaps is expected to provide a reasonable approximation but does not fully capture the complex interactions between

775 meteorology, atmospheric stability, grazing activity, urination patterns, deposition spatial heterogeneity and background exchange. To some extent, the difficulty in explaining the variations in EF between grazing events is also a reflection of the uncertainty in gap-filling. EF values, as the most synthetic, high-level product of the study, combine all the individual uncertainties of lower-level variables and should be interpreted with caution.

Ammonia emissions from grazed grasslands vary significantly between studies not only due to differences in management and

780 environmental factors but also due to potential differences and biases between measurement techniques. Early mass balance methods (e.g., integrated horizontal flux using filter packs) lacked the temporal resolution needed to resolve short-term grazing emissions, requiring extensive manual sampling. Automated higher frequency measurement techniques, such as quantum cascade laser spectroscopy, wet denuder with online analysis or miniDOAS applied to eddy covariance, AGM or backward Lagrangian stochastic (bLS) inversion, have advanced NH_3 flux monitoring. Nevertheless, methodological inconsistencies still

785 limit cross-study comparisons, as was shown by Sintermann et al. (2012) in the case of field slurry spreading. While no universal standard for NH_3 flux measurements currently exists, recent advancements in open-path eddy covariance (EC) methods may help address limitations in existing techniques (Swart et al., 2023).

Paired miniDOAS systems with bLS have been applied to grazed grasslands (Bell et al. 2017; Volgmeier et al., 2018). Laubach et al. (2013) used a mass balance approach, while Laubach et al. (2012) focused on artificial urine patch studies. The fluxes

790 and EF observed at the field scale in this study align with those of Volgmeier et al. (2018) and Bell et al. (2017) in similar-sized fields (~1-2 ha). Smaller paddocks may tend to yield higher NH_3 fluxes due to concentrated grazing and higher excretion density, while larger fields may dilute emissions. The largest cattle-based EF reported in Table 4 was obtained from measurements conducted in small demarcated fields (<0.1 ha) with livestock provided with a mixed diet (rye-grass clover mixture).

795 Vegetation type and fertilization history significantly influence NH_3 fluxes. Our study site was dominated by ryegrass, whereas other studies included mixed swards with legumes such as white clover, which can alter nitrogen cycling and urinary composition. Bussink (1992), demonstrated that excessive fertilization (550 kg N ha^{-1}) increased NH_3 volatilisation due to higher urinary N content. Jarvis et al. (1989a) compared fertilized ryegrass monocultures and unfertilized ryegrass-clover pastures over two years and found that, while the mean cattle head-based EF across both years was lower for the unfertilized

800 ryegrass-clover mixture, the second year showed a higher cattle head-based EF for the unfertilized ryegrass-clover mixture than for the 210 kg N ha^{-1} fertilized ryegrass. The average emitted fraction of deposited N was also higher in the unfertilized rye-grass clover mixture compared to the 210 kg N ha^{-1} fertilized ryegrass. These findings suggest that biological nitrogen fixation and associated changes in urine composition may contribute to increased NH_3 emissions under certain conditions.

The management of the experimental site in this study frequently includes organic and mineral fertilization, as well as occasional cutting events for hay or silage harvest. Emissions from grass cuts can be comparable to grazing (Milford et al., 2009), while Spirig et al. (2010), reported peak NH_3 emissions from slurry application reaching 70000 ng m^{-2} s^{-1}, twenty times larger than peak grazing fluxes in this study. This highlights the importance of considering fertilization type, application method, and all other aspects and fluxes related to pasture management if the goal is to describe total net NH_3 emissions from the entire grazed, fertilized, cut grassland system, not just emissions occurring during grazing phases.

Table 4: Comparison of NH$_3$ fluxes, grazing event-based emission factors (EFs) and measurement methodologies in studies of grazed grassland studies. Mixed vegetation refers to grasslands with a ryegrass-clover sward.

Reference	Country	Year, month (N days)	Vegetation (grazing management)	Annual N Fertilizer kg N ha⁻¹ yr⁻¹ (type)	Stocking density LSU ha⁻¹ (field size in ha)	Method	Resolution	Flux Valid Data (%)	Flux range min | max ng NH₃ m⁻² s⁻¹	EF g NH₃-N cow⁻¹ grazing d⁻¹ (% relative to excreted-urine N) Range min | max	Mean/Med
This Study	France	2021-2024, 03-06 (5-10)	Ryegrass (F, +C)	166 (AN+S)	16-55(2.35)	AGM	30 min	35-68	-113 | 3205	1.1 (1) | 23.3 (20)	7.8 (7) μA; 2.9 (4)med; 4.2 (5)μG
Voglmeier et al., 2018	Switzerland	2016, 05-09, (3-5)	Mixed (P, +C); Mixed (F, -C)	120	71 (0.17); 55 (0.22)	MD-bLS	30 min	34-65; 30-50	0 | 2550; 0 | 2793	(5) | (11); (7) | (16)	12.8 ± 2.2 (7)μA; 21.4 ± 1.2 (10)μA
Bell et al., 2017	France	2015, 05 (3-6)	Mixed (F, -C)	150	22-44 (1.98)	MD-bLS	30 min	42-65	-100 | 1000	5.4 (4) | 5.9 (10)	5.8 ± 1.7 (7)μA
Möring et al., 2017	Scotland, UK	2002, 08-09; 2003, 06	Ryegrass	na	3-10 (5.42)	AGM	1 hr	na	-100 | 180	na	na
Laubach et al., 2013	New Zealand	2011, 03 (10)	Mixed (H, -C)	na	150 (0.08)	IHF	30 min	na	0 | 15300	na	53.9 (22.4*)
Bussink, 1992	The Netherlands	1987, 05-10; 1988, 04 -10	Ryegrass (F, -C)	550(CAN); 550(CAN); 250(CAN)	60-120 (0.18)	IHF	6-hrs	na	0 | 5500	22.6 (5*) | 73.2 (15*); 4.4 (1*) | 82.2 (13*); 6.2 (2*) | 27.9 (6*)	46.5 (9*)μA; 40.2 (8*) μA; 14.0 (3*) μA
Jarvis et al., 1989a, b	UK	1986, 04-10; 1987, 05-10	Ryegrass (+H, -C); Ryegrass (+H, -C); Mixed (+H, -C)	420(AN); 210(AN); 0	16-65 (0.12)	IHF	24-hrs	na	na	11.0 | 19.0; 7.0 | 10.0; 1.0 | 10.0	16.0 (12) μA; 8.5 (5)μA; 5.5 (7)μA

μA:arithmetic mean; μG: geometric mean; med: median
N days: Duration considered to compute EF after cattle departure
Pasture management: F full-time grazing, P part-time grazing, H Harvested pasture
Grazing with other diet complementation (+C), without (-C)
Fertilization: S Slurry, AN ammonium nitrate, CAN calcium ammonium nitrate
Measurement methods: MD-bLS refers to Mini-DOAS combined with bLS backward Lagrangian stochastic model, IHF integrated horizontal flux
*: (% relative to total excreted-N as urine and dung)

5 Conclusion

820 Long-term, high-resolution NH_3 flux monitoring datasets across diverse grazing systems and under different climatic conditions are essential for improving process understanding, refining emission estimates and reducing uncertainty in national and global emission inventories. This study presents one of the most extensive high-resolution datasets of field-scale grazing-induced NH_3 fluxes, capturing diurnal, seasonal and inter-annual variability. The data show that grazing in intensively managed grasslands can contribute cumulative seasonal fluxes magnitudes larger than emissions from applied mineral fertilizers and

825 potentially even organic fertilizers, depending on stocking density, vegetation characteristics, and meteorological conditions. The data indicate a very large variability in time-integrated emission factors per livestock unit between eight grazing events, rather at the low end of the range of values from the few other datasets found in the literature. Thus, they highlight the difficulty of generalizing the results to national or continental scales. These differences underscore the role of site-specific conditions (meteorology, soil) and livestock management practices on NH_3 emissions.

830 Despite the extensive flux data coverage across four years and contrasting environmental conditions at our site, the EF variability could not be explained by the available data for the most likely meteorological, ecosystem and management drivers. Untangling the relative share of control by individual control factors through correlation analysis is practically impossible on the sole basis of in-situ field observations, partly due to cross-correlations between drivers. This is also very likely partly due to the large uncertainties in measurement-derived EF estimates, which combine a long chain of random errors in individual

835 measured variables, systematic errors in AGM (NH_3 sampling, advection, concentration footprint and uncertainties in Monin Obukhov similarity theory), field-scale grazing heterogeneity, correction procedures (flux footprint attribution), and finally gap-filling methodology. Process-based models offer a potential alternative to average or default EF values for upscaling, but require robust observational datasets for calibration and validation. Future research should focus on i) continued long-term NH_3 flux monitoring in grazed grasslands in diverse situations using state-of-the-art methodology (e.g., open-path eddy

840 covariance), and ii) incorporating soil-vegetation-animal-atmosphere interactions into process-based models to improve NH_3 emission predictions, and to provide mechanism-based EF for spatial and temporal generalization and prospective studies.

6 Code and data availability

The code used for gap filling will be published on Zenodo but can be requested from M.O. Abdulwahab (Mubaraq-olarewaju.abdulwahab@inrae.fr). Data can also be requested from C. Flechard (Christophe.flechard@inrae.fr).

7 Author Contributions

The original draft was prepared by MOA and CF, with input and contributions from all co-authors. YF carried out all NH_3 denuder chemical analyses, as well as those performed on soil and plant samples. In-situ sampling, data collection and laboratory sample preparations were carried out by MOA, YF, CF, AJ and PB. Data analysis, interpretation, and curation were conducted by MOA, CF and YF with expert guidance on flux calculations and footprint analysis by AN and CH. Funding acquisition and project management were dealt with by NE and CF. PhD project supervision was provided by VV, CF and AIG. All authors participated in the critical review and editing of the manuscript.

8 Supplementary materials

Supplementary materials related to this article have been submitted.

9 Competing interests

The authors declare no conflict of interest.

10 Acknowledgement

This work was mainly carried out within the CORTEA-EMIGRAZE and the EU-Horizon2020 CCCfarming (grant agreement n° 696231) research projects, funded by the French Agency for Ecological Transition (ADEME) and the French National Research Agency (ANR), respectively. The PhD studentship of M.O. Abdulwahab was co-funded by the Région Bretagne regional council's ARED grant and by INRAE's Agroecosystem Department. We acknowledge funding by Rennes Métropole City Council's AIS scheme, by ADEME, and by the Observatoire des sciences de l'environnement de Rennes (OSEREN), which contributed to the acquisition of the Los Gatos Research analyser. The ICOS flux tower equipment was co-funded by the CPER Buffon and CPER AgroEcoTerMer funding initiatives for environmental instrumentation, supported by the French State and the European Regional Development Fund (ERDF) through Région Bretagne. Financial support was also provided by the ICOS-France research infrastructure, and we are grateful to the European ICOS Research Infrastructure for hosting and providing access to, the FR-Mej dataset (https://doi.org/10.18160/G5KZ-ZD83). We gratefully acknowledge the help and assistance of all staff at the INRAE-IEPL experimental farm (Méjusseaume, Le Rheu, France), in particular Gaël Boullet regarding herd and grazing management, Arnaud Mottin for biomass sampling and measurements, and Jérémy Eslan who designed and built the vertical sampling lift system at the IEPL workshop. We also thank Rémy Delegarde who provided the data used to compute the urinary N content.

11 References

Anderson, R. G., Yates, S. R., Ashworth, D. J., Jenkins, D.L., and Zhang, Q.: Reducing the discrepancies between the aerodynamic gradient method and other micrometeorological approaches for measuring fumigant emissions. Sci. Total Environ., 687, 392–400, 2019.

875   Asman, W. A. H., Sutton, M. A., and Schjørring, J. K.: Ammonia: Emission, atmospheric transport and deposition, New Phytol., 139, 27–48, https://doi.org/10.1046/j.1469-8137.1998.00180.x, 1998.

Bell, M., Flechard, C., Fauvel, Y., Häni, C., Sintermann, J., Jocher, M., Menzi, H., Hensen, A., and Neftel, A.: Ammonia emissions from a grazed field estimated by miniDOAS measurements and inverse dispersion modelling, Atmos. Meas. Tech., 10, 1875–1892, https://doi.org/10.5194/amt-10-1875-2017, 2017.

880   Brümmer, C., Rüffer, J. J., Delorme, J.-P., Wintjen, P., Schrader, F., Beudert, B., Schaap, M., and Ammann, C.: Reactive nitrogen fluxes over peatland and forest ecosystems using micrometeorological measurement techniques, Earth Syst. Sci. Data, 14, 743–761, https://doi.org/10.5194/essd-14-743-2022, 2022.

Bussink, D. W.: Ammonia volatilization from grassland receiving nitrogen fertilizer and rotationally grazed by dairy cattle. Fert. Res., 33, 257–265, https://doi.org/10.1007/BF01050881, 1992.

885   Carozzi, M., Loubet, B., Acutis, M., Rana, G., and Ferrara, R. M.: Inverse dispersion modelling highlights the efficiency of slurry injection to reduce ammonia losses by agriculture in the Po Valley (Italy), Agric. For. Met., 171–172, 306–318, https://doi.org/10.1016/j.agrformet.2012.12.012, 2013.

Csavina, J., Roberti, J. A., Taylor, J. R., and Loescher, H. W.: Traceable measurements and calibration: A primer on uncertainty analysis. Ecosphere, 8, e01683, https://doi.org/10.1002/ecs2.1683, 2017.

890   Denmead, O. T., Freney, J. R., and Simpson, J. R.: A closed ammonia cycle within a plant canopy, Soil Biol. Biochem., 8, 161–164, https://doi.org/10.1016/0038-0717(76)90083-3, 1976.

Dyer, A., and Hicks, B.: Flux-gradient relationships in the constant flux layer. Quart. J. Roy. Met. Soc., 96, 715–721, https://doi.org/10.1002/qj.49709641012, 1970.

European Environment Agency (EEA): Industrial Reporting under the Industrial Emissions Directive 2010/75/EU and
895   European Pollutant Release and Transfer Register Regulation (EC) No 166/2006, https://www.eea.europa.eu/data-and-maps/data/industrial-reporting-under-the-industrial-6 (last access: 2 April 2025), 2022.

Ellis, R. A., Murphy, J. G., Pattey, E., van Haarlem, R., O'Brien, J. M., and Herndon, S. C.: Characterizing a Quantum Cascade Tunable Infrared Laser Differential Absorption Spectrometer (QC-TILDAS) for measurements of atmospheric ammonia, Atmos. Meas. Tech., 3, 397–406, https://doi.org/10.5194/amt-3-397-2010, 2010.

900   Famulari, D., Fowler, D., Hargreaves, K., Milford, C., Nemitz, E., Sutton, M. A., and Weston, K.: Measuring eddy covariance fluxes of ammonia using tunable diode laser absorption spectroscopy, Water Air Soil Poll. Focus, 4, 151–158, https://doi.org/10.1007/s11267-005-3025-9, 2005.

FAO: World Food and Agriculture – Statistical Yearbook 2023, Food and Agriculture Organization of the United Nations, Rome, https://openknowledge.fao.org/handle/20.500.14283/cc8166en (last access: 1 April 2025), 2023.

905   Ferm, M.: Method for determination of atmospheric ammonia, Atmos. Environ., 13, 1385–1393, https://doi.org/10.1016/0004-6981(79)90107-0, 1979.

Finkelstein, P. L., and Sims, P. F.: Sampling error in eddy correlation flux measurements, Journal of Geophysical Research, 106, 3503, https://doi.org/10.1029/2000JD900731, 2001.

Flechard, C. R., and Fowler, D.: Atmospheric ammonia at a moorland site. II: Long-term surface-atmosphere
910   micrometeorological flux measurements, Quart. J. Roy. Met. Soc., 124, 759–791, https://doi.org/10.1002/qj.49712454706, 1998.

Flechard, C. R., Massad, R.-S., Loubet, B., Personne, E., Simpson, D., Bash, J. O., Cooter, E. J., Nemitz, E., and Sutton, M. A.: Advances in understanding, models and parameterizations of biosphere-atmosphere ammonia exchange, Biogeosciences, 10, 5183–5225, https://doi.org/10.5194/bg-10-5183-2013, 2013.

915   Flechard, C. R., Spirig, C., Neftel, A., and Ammann, C.: The annual ammonia budget of fertilised cut grassland – Part 2: Seasonal variations and compensation point modeling, Biogeosciences, 7, 537–556, https://doi.org/10.5194/bg-7-537-2010, 2010.

Flesch, T. K., Prueger, J. H., and Hatfield, J. L.: Turbulent Schmidt number from a tracer experiment, Agric. For. Met., 111, 299–307, https://doi.org/10.1016/S0168-1923(02)00025-4, 2002.

920   Foken, T.: 50 years of the Monin-Obukhov similarity theory, Bound.-Lay. Meteorol., 119, 431–447, https://doi.org/10.1007/s10546-006-9048-6, 2006.

Forster, P., Storelvmo, T., Armour, K., Collins, W., Dufresne, J., Frame, D., Lunt, D., Mauritsen, T., Palmer, M., and Watanabe, M.: The Earth's energy budget, climate feedbacks, and climate sensitivity, in: Climate Change 2021: The Physical Science Basis, Contribution of Working Group I to the Sixth Assessment Report of the Intergovernmental
925   Panel on Climate Change, edited by: Masson-Delmotte, V., Zhai, P., Pirani, A., Connors, S. L., Péan, C., Berger, S., et al., Cambridge University Press, Cambridge, United Kingdom and New York, NY, USA, https://doi.org/10.1017/9781009157896.009, 2021.

Fowler, D. and Duyzer, J. H.: Micrometeorological techniques for the measurement of trace gas exchange, in: Exchange of Trace Gases Between Terrestrial Ecosystems and the Atmosphere, edited by: Andreae, M. O. and Schimel, D. S.,
930   Wiley, Chichester, 189–207, 1989.

Freney, J. R., Simpson, J. R., and Denmead, O. T.: Volatilization of ammonia, in: Gaseous Loss of Nitrogen from Plant-Soil Systems, edited by: Freney, J. R. and Simpson, J. R., Springer Netherlands, 1-32, https://doi.org/10.1007/978-94-017-1662-8_1, 1983.

Giltrap, D., Saggar, S., Rodriguez, J., and Bishop, P.: Modelling NH$_3$ volatilisation within a urine patch using NZ-DNDC,
935   Nutr. Cycl. Agroecosyst., 108, 267–277, https://doi.org/10.1007/s10705-017-9854-x, 2017.

Häni, C., Neftel, A., Flechard, C., Ammann, C., Valach, A., and Kupper, T.: Validation of a short-range dispersion and deposition model using field-scale ammonia and methane release experiments, Agric. For. Met., 353, 110041. https://doi.org/10.1016/j.agrformet.2024.110041, 2024.

Harper, L. A.: Ammonia: Measurement issues, in: Micrometeorology in Agricultural Systems, Agronomy Monograph, 47,
940   edited by: Hatfield, J. L. and Baker, J. M., ASA-CSSA-SSSA, Madison, WI, 345–379, 2005.

Harper, L. A., Catchpoole, V. R., Davis, R., and Weir, K. L.: Ammonia volatilization: soil, plant, and microclimate effects on diurnal and seasonal fluctuations, Agronomy Journal, 75, 212–218, https://doi.org/10.2134/agronj1983.00021962007500020014x, 1983.

Högström, U.: Non-dimensional wind and temperature profiles in the atmospheric surface layer: A re-evaluation, Bound.-Lay.
945   Meteorol., 42, 55–78, https://doi.org/10.1007/BF00119875, 1988.

Högström, U.: Review of some basic characteristics of the atmospheric surface layer, Bound.-Lay. Meteorol., 78, 215–246, https://doi.org/10.1007/BF00120937, 1996.

Hristov, A. N., Hanigan, M., Cole, A., Todd, R., McAllister, T. A., Ndegwa, P. M., and Rotz, A.: Review: Ammonia emissions from dairy farms and beef feedlots, Can. J. Anim. Sci., 91, 1–35, https://doi.org/10.4141/CJAS10034, 2011.

950   Jarvis, S. C., Hatch, D. J., and Lockyer, D. R.: Ammonia fluxes from grazed grassland: Annual losses from cattle production systems and their relation to nitrogen inputs, J. Agric. Sci., 113, 99–108, https://doi.org/10.1017/S0021859600084677, 1989a.

Jarvis, S. C., Hatch, D. J., Orr, R. J., and Reynolds, S. E.: Micrometeorological studies of ammonia emission from sheep grazed swards, J. Agric. Sci., 117, 101–109. https://doi.org/10.1017/S0021859600079028, 1991.

955   Jarvis, S. C., Hatch, D. J., and Roberts, D. H.: The effects of grassland management on nitrogen losses from grazed swards through ammonia volatilization; the relation to excretal N returns from cattle, J. Agric. Sci., 112, 205–216, https://doi.org/10.1017/S0021859600085117, 1989b.

Kamp, J. N., Häni, C., Nyord, T., Feilberg, A., and Sørensen, L. L.: The aerodynamic gradient method: implications of non-simultaneous measurements at alternating heights, Atmosphere, 11, https://doi.org/10.3390/atmos11101067, 2020.

960   Kamp, J. N., Häni, C., Nyord, T., Feilberg, A., and Sørensen, L. L.: Calculation of NH_3 emissions, evaluation of backward lagrangian stochastic dispersion model and aerodynamic gradient method, Atmosphere, 12, https://doi.org/10.3390/atmos12010102, 2021, 2021.

Kormann, R., and Meixner, F. X.: An analytical footprint model for non-neutral stratification, Bound.-Lay. Meteorol., 99, 207–224, https://doi.org/10.1023/A:1018991015119, 2001.

965   Laubach, J., Taghizadeh-Toosi, A., Sherlock, R. R., and Kelliher, F. M.: Measuring and modelling ammonia emissions from a regular pattern of cattle urine patches, Agric. For. Met., 156, 1-17, 2012.

Laubach, J., Taghizadeh-Toosi, A., Gibbs, S., Sherlock, R., Kelliher, F. M., and Grover, S.: Ammonia emissions from cattle urine and dung excreted on pasture, Biogeosciences, 10, 327–338, 2013.

Leen, J. B., Yu, X.-Y., Gupta, M., Baer, D. S., Hubbe, J. M., Kluzek, C. D., Tomlinson, J. M., and Hubbell, M. R.: Fast in
970   situ airborne measurement of ammonia using a mid-infrared off-axis ICOS spectrometer, Environ. Sci. Technol., 47,
10446–10453, 2013.

Loubet, B., Cellier, P., Fléchard, C., Zurfluh, O., Irvine, M., Lamaud, E., Stella, P., Roche, R., Durand, B., Flura, D., Masson,
S., Laville, P., Garrigou, D., Personne, E., Chelle, M., and Castell, J.-F.: Investigating discrepancies in heat, CO_2
fluxes and O_3 deposition velocity over maize as measured by the eddy-covariance and the aerodynamic gradient
975   methods, Agric. For. Met., 169, 35–50, https://doi.org/10.1016/j.agrformet.2012.09.010, 2013.

Loubet, B., Decuq, C., Personne, E., Massad, R. S., Flechard, C., Fanucci, O., Mascher, N., Gueudet, J.-C., Masson, S., Durand,
B., Genermont, S., Fauvel, Y., and Cellier, P.: Investigating the stomatal, cuticular and soil ammonia fluxes over a
growing tritical crop under high acidic loads, Biogeosciences, 9, 1537–1552, https://doi.org/10.5194/bg-9-1537-
2012, 2012.

980 Loubet, B., Milford, C., Hill, P. W., Tang, Y. S., Cellier, P., and Sutton, M. A.: Seasonal variability of apoplastic NH_4^+ and
pH in an intensively managed grassland, Plant and Soil, 238, 97–110, https://doi.org/10.1023/A:1014208926195,
2002.

Luo, J., Wyatt, J., van der Weerden, T. J., Thomas, S. M., de Klein, C. A. M., Li, Y., Rollo, M., Lindsey, S., Ledgard, S. F.,
Li, J., Ding, W., Qin, S., Zhang, N., Bolan, N., Kirkham, M. B., Bai, Z., Ma, L., Zhang, X., Wang, H., … Rys, G.:
985   Potential hotspot areas of nitrous oxide emissions from grazed pastoral dairy farm systems in: Advances in
Agronomy,145, edited by: Sparks, D. L., Academic Press, 205–268, https://doi.org/10.1016/bs.agron.2017.05.006,
2017.

Massad, R. S., Tuzet, A., Personne, E., Bedos, C., Beekmann, M., Coll, I., Drouet, J.-L., Fortems-Cheiney, A., Génermont, S.,
and Loubet, B.: Modelling exchanges: From the process scale to the regional scale, in: Agriculture and Air Quality:
990   Investigating, Assessing and Managing, edited by: Loubet, B., Cellier, P., Génermont, S., and Sutton, M. A., Springer,
Cham, 159–207, 2020.

Massad, R. S., Nemitz, E., and Sutton, M. A.: Review and parameterisation of bi-directional ammonia exchange between
vegetation and the atmosphere, Atmos. Chem. Phys., 10, 10359–10386. https://doi.org/10.5194/acp-10-10359-2010,
2010.

995 Mauder, M., Foken, T., Aubinet, M., and Ibrom, A.: Eddy-covariance measurements, in: Springer Handbook of Atmospheric
Measurements edited by: Foken, T., Springer International Publishing, 1473–1504, https://doi.org/10.1007/978-3-
030-52171-4_55, 2021.

Mauder, M. and Foken, T.: Documentation and instruction manual of the Eddy Covariance software package TK2, Univ
Bayreuth, Abt Mikrometeorol., 26–42, available at: https://epub.uni-bayreuth.de/884/1/ARBERG026.pdf (last
1000   access: 27 March 2025), 2004.

Melman, E. A., Rutledge-Jonker, S., Braam, M., Frumau, K. F. A., Moene, A. F., Shapkalijevski, M., and van Zanten, M. C.: Increasing complexity in Aerodynamic Gradient flux calculations inside the roughness sublayer applied on a two-year dataset, Agric. For. Met., 355, 110107, https://doi.org/10.1016/j.agrformet.2024.110107, 2024.

Milford, C., Theobald, M. R., Nemitz, E., Hargreaves, K. J., Horvath, L., Raso, J., Dämmgen, U., Neftel, A., Jones, S. K., Hensen, A., Loubet, B., Cellier, P., and Sutton, M. A.: Ammonia fluxes in relation to cutting and fertilization of an intensively managed grassland derived from an inter-comparison of gradient measurements, Biogeosciences, 6, 819–834, https://doi.org/10.5194/bg-6-819-2009, 2009.

Milford, C., Theobald, M. R., Nemitz, E., and Sutton, M. A.: Dynamics of ammonia exchange in response to cutting and fertilising in an intensively-managed grassland, Water, Air and Soil Poll. Focus, 1, 167–176. https://doi.org/10.1023/A:1013142802662, 2001.

Mitchell, E., De Rosa, D., Grace, P., and Rowlings, D.: Herd concentration areas create greenhouse gas hotspots, Nutr. Cycl. Agroecosyst., 121, 15–26, https://doi.org/10.1007/s10705-021-10159-0, 2021.

Monteith, J. L. and Unsworth, M. H.: Principles of Environmental Physics, 2nd edn., Edward Arnold, London, 291 pp., ISBN 9780340662770, 1990.

Móring, A., Vieno, M., Doherty, R. M., Milford, C., Nemitz, E., Twigg, M. M., Horváth, L., and Sutton, M. A.: Process-based modelling of NH_3 exchange with grazed grasslands, Biogeosciences, 14, 4161–4193, https://doi.org/10.5194/bg-14-4161-2017, 2017.

Nemitz, E., Milford, C., and Sutton, M. A.: A two-layer canopy compensation point model for describing bi-directional biosphere-atmosphere exchange of ammonia, Quart. J. Roy. Met. Soc., 127, 815–833, https://doi.org/10.1002/qj.49712757306, 2001.

Nemitz, E., Sutton, M. A., Wyers, G. P., and Jongejan, P. A. C.: Gas-particle interactions above a Dutch heathland: I. Surface exchange fluxes of NH_3, SO_2, HNO_3 and HCl, Atmos. Chem. Phys., 4, 989–1005, https://doi.org/10.5194/acp-4-989-2004, 2004.

Panofsky, H. A.: Determination of stress from wind and temperature measurements, Quart. J. Roy. Met. Soc., 89, 85–94, 1963.

Paulson, C. A.: The mathematical representation of wind speed and temperature profiles in the unstable atmospheric surface layer, J. Appl. Meteorol., 857–861, 1970.

Reynolds, C. and Wolf, D.: Influence of urease activity and soil properties on ammonia volatilization from urea, Soil Sci., 143, 418–425, 1987.

Riedo, M., Milford, C., Schmid, M., and Sutton, M. A.: Coupling soil–plant–atmosphere exchange of ammonia with ecosystem functioning in grasslands, Ecol. Model., 158, 83–110, https://doi.org/10.1016/S0304-3800(02)00169-2, 2002.

Salmon, G. R., MacLeod, M., Claxton, J., Ciamarra, U. P., Robinson, T., Duncan, A., and Peters, A.: Exploring the landscape of livestock 'facts', Glob. Food Sec., 25, https://doi.org/10.1016/j.gfs.2019.100329, 2020.

1035   Schulte, R. B., Vilà-Guerau de Arellano, J., Rutledge-Jonker, S., van der Graaf, S., Zhang, J., and van Zanten, M. C.:
             Observational relationships between ammonia, carbon dioxide and water vapor under a wide range of meteorological
             and turbulent conditions: RITA-2021 campaign, Biogeosciences, 21, 557–574, https://doi.org/10.5194/bg-21-557-
             2024, 2024.

         Selbie, D. R., Buckthought, L. E., and Shepherd, M. A.: The Challenge of the Urine Patch for Managing Nitrogen in Grazed
1040   Pasture Systems, in: Advances in Agronomy, Vol. 129, edited by: Sparks, D. L.   Elsevier, 229-292,
             https://doi.org/10.1016/bs.agron.2014.09.004, 2015.

         Sintermann, J., Neftel, A., Ammann, C., Häni, C., Hensen, A., Loubet, B., and Flechard, C. R.: Are ammonia emissions from
             field-applied slurry substantially over-estimated in European emission inventories? Biogeosciences, 9, 1611–1632,
             https://doi.org/10.5194/bg-9-1611-2012, 2012.

1045   Skiba, U., Pitcairn, C., Sheppard, L., Kennedy, V., and Fowler, D.: The influence of atmospheric N deposition on nitrous oxide
             and nitric oxide fluxes and soil ammonium and nitrate concentrations, Water, Air, & Soil Poll. Focus, 4, 37–43,
             https://doi.org/10.1007/s11267-005-3011-2, 2005.

         Sommer, S. G., Schjoerring, J. K., and Denmead, O. T.: Ammonia emission from mineral fertilizers and fertilized crops, in:
             Advances in Agronomy, Vol. 82, edited by: Sparks, D. L., Elsevier, 557–622, https://doi.org/10.1016/S0065-
1050   2113(03)82008-4, 2004, 2004.

         Sommer, S. G., Webb, J., and Hutchings, N. D.: New emission factors for calculation of ammonia volatilization from European
             livestock manure management systems, Front. Sustain. Food Syst., 3, https://doi.org/10.3389/fsufs.2019.00101, 2019.

         Sommer, S., Génermont, S., Cellier, P., Hutchings, N., Olesen, J., and Morvan, T.: Processes controlling ammonia emission
             from livestock slurry in the field, Eur. J. Agron., 19, 465–486, 2003.

1055   Spirig, C., Flechard, C. R., Ammann, C., and Neftel, A.: The annual ammonia budget of fertilised cut grassland – Part 1:
             Micrometeorological flux measurements and emissions after slurry application, Biogeosciences, 7, 521–536.
             https://doi.org/10.5194/bg-7-521-2010, 2010.

         Stull, R. B.: An introduction to boundary layer meteorology, Atmospheric and Oceanographic Sciences Library, Vol. 13,
             Springer, Dordrecht, 670 pp., ISBN 9789400930278, 2012.

1060   Sutton, M. A., Howard, C. M., Erisman, J. W., Billen, G., Bleeker, A., Grennfelt, P., van Grinsven, H., and Grizzetti, B. (Eds.):
             The European nitrogen assessment: sources, effects and policy perspectives, Cambridge University Press, Cambridge,
             612 pp., https://doi.org/10.1017/CBO9780511976988, 2011.

         Sutton, M. A., Reis, S., Riddick, S. N., Dragosits, U., Nemitz, E., Theobald, M. R., Tang, Y. S., Braban, C. F., Vieno, M., and
             Dore, A. J.: Towards a climate-dependent paradigm of ammonia emission and deposition, Philos. Transact. R. Soc.
1065   B, 368, 20130166, https://doi.org/10.1098/rstb.2013.0166, 2013.

         Sutton, M. A., Tang, Y. S., Miners, B., and Fowler, D.: A new diffusion denuder system for long-term, regional monitoring of
             atmospheric ammonia and ammonium. in: Air-Surface Exchange of Gases and Particles, edited by: Fowler, D.,

Pitcairn, C., and Erisman, J.-W., Springer Netherlands, 145–156, https://doi.org/10.1007/978-94-010-9026-1_15, 2001.

1070 Sutton, M. A. and Fowler, D.: Dry deposition of ammonia to frozen land surfaces and analysis of the uncertainties in fluxes deriving from measurement errors, Pap. COST 611 Workshop, Development of Analytical Techniques for Atmospheric Measurements, Rome, April 1992, CEC, Brussels, 1992.

Sutton, M., Fowler, D., Moncrieft, J., and Storeton-West, R.: The exchange of atmospheric ammonia with vegetated surfaces. II: Fertilized vegetation. Quart. J. Roy. Met. Soc., 119, 1047–1070, 1993.

1075 Sutton, M. A., Howard, C. M., Mason, K. E., Brownlie, W. J., and Cordovil, C. M. d. S.: Nitrogen opportunities for agriculture, food and environment: UNECE guidance document on integrated sustainable nitrogen management, UK Center for Ecology & Hydrology, Edinburgh, UK, 157 pp., ISBN 978-1-906698-78-2, https://unece.org/environment-policy/publications/guidance-document-integrated-sustainable-nitrogen-management (last access: 3 April 2025), 2022.

1080 Swart, D., Zhang, J., van der Graaf, S., Rutledge-Jonker, S., Hensen, A., Berkhout, S., Wintjen, P., van der Hoff, R., Haaima, M., Frumau, A., van den Bulk, P., Schulte, R., van Zanten, M., and van Goethem, T.: Field comparison of two novel open-path instruments that measure dry deposition and emission of ammonia using flux-gradient and eddy covariance methods, Atmos. Meas. Tech., 16, 529–546, https://doi.org/10.5194/amt-16-529-2023, 2023.

Thom, A. S.: Momentum, mass and heat exchange of plant communities, in: Vegetation and the Atmosphere, Vol. 1, edited
1085 by: Monteith, J.L., Academic Press, London, 57–109, 1975.

Vallis, I., Harper, L., Catchpoole, V., and Weier, K.: Volatilization of ammonia from urine patches in a subtropical pasture, Aust. J. Agric. Res., 33, 97–107, 1982.

Voglmeier, K., Jocher, M., Häni, C., and Ammann, C.: Ammonia emission measurements of an intensively grazed pasture, Biogeosciences, 15, 4593–4608, https://doi.org/10.5194/bg-15-4593-2018, 2018.

1090 .Walker, J. T., Jones, M. R., Bash, J. O., Myles, L., Meyers, T., Schwede, D., Herrick, J., Nemitz, E., and Robarge, W.: Processes of ammonia air–surface exchange in a fertilized *Zea mays* canopy, Biogeosciences, 10, 981–998, https://doi.org/10.5194/bg-10-981-2013, 2013.

Webb, E. K.: Profile relationships: The log-linear range, and extension to strong stability. Quart. J. Roy. Met. Soc., 96, 67–90, 1970.

1095 Whitehead, D. C., and Raistrick, N.: The volatilization of ammonia from cattle urine applied to soils as influenced by soil properties, Plant Soil, 148, 43–51, https://doi.org/10.1007/BF02185383, 1993.

Whitehead, J. D., Twigg, M., Famulari, D., Nemitz, E., Sutton, M. A., Gallagher, M. W., and Fowler, D.: Evaluation of laser absorption spectroscopic techniques for eddy covariance flux measurements of ammonia, Environ. Sci. Technol., 42, 2041–2046, https://doi.org/10.1021/es071596u, 2008.

1100 Wichink Kruit, R. J., van Pul, W. A. J., Otjes, R. P., Hofschreuder, P., Jacobs, A. F. G., and Holtslag, A. A. M.: Ammonia fluxes and derived canopy compensation points over non-fertilized agricultural grassland in the Netherlands using

the new gradient ammonia—High accuracy—Monitor (GRAHAM), Atmos, Environ., 41, 1275–1287, https://doi.org/10.1016/j.atmosenv.2006.09.039, 2007.

Wilson, J. D.: Turbulent Schmidt numbers above a wheat crop, Bound.-Lay. Meteorol., 148, 255–268, https://doi.org/10.1007/s10546-013-9819-9, 2013.

1105